Lawrence Berkeley National Laboratory

Title
Experimental estimation of the bisulfite isomer quotient as a function of temperature: Implications for sulfur isotope fractionations in aqueous sulfite solutions

Permalink
https://escholarship.org/uc/item/7bb6q2wt

Authors
Eldridge, Daniel L
Mysen, Bjorn O
Cody, George D

Publication Date
2018

DOI
10.1016/j.gca.2017.10.005

Peer reviewed

Experimental estimation of the bisulfite isomer quotient as a function of temperature: Implications for sulfur isotope fractionations in aqueous sulfite solutions

Daniel L. Eldridge *, Bjorn O. Mysen, George D. Cody

Geophysical Laboratory, Carnegie Institution of Washington, 5251 Broad Branch Road NW, Washington, DC 20015, United States

Abstract

Bisulfite (HSO_3^-) and sulfite (SO_3^{2-}) compounds play key roles in numerous geochemical and biochemical processes extending from the atmosphere to the subseafloor biosphere. Despite decades of spectroscopic investigations, the molecular composition of HSO_3^- in solution remains uncertain and, thus, the role of bisulfite in (bio)chemical and isotope fractionation processes is unclear. We report new experimental estimates for the bisulfite isomer quotient ($Q_i = [(HO)SO_2^-]/[(HS)O_3^-]$; [] = concentration) as a function of temperature from the interpretation of Raman spectra collected from aqueous $NaHSO_3$ solutions contained in fused silica capsules. In pure $NaHSO_3$ solutions ($1Na^+:1HSO_3^-$, stoichiometric) over $[NaHSO_3]$ = 0.2–0.4 m (moles/kg H_2O), the following relationship is obtained:

$$\ln(Q_i) = \frac{878.59(\pm 32.98)}{T} - 1.9642(\pm 0.1081),$$

where T = 278–358 K (5–85 °C) (based on 50 determinations; additional significant figures are provided to avoid rounding errors). This relationship suggests that the minor isomer, $(HS)O_3^-$, may comprise 23–38% ($\pm 3\%$) of the mole fraction of HSO_3^- over 5–85 °C, respectively, which is higher in relative abundance than has generally been understood previously. We additionally provide estimates for Q_i in $NaHSO_3$ solutions containing a total ionic strength of μ = 1.0 m (0.2 m $NaHSO_3$ + 0.8 m NaCl) and different pH (3.3–4.5), but do not appear to resolve any significant differences in Q_i as a function of these additional variables. These new values of Q_i are employed to re-assess the bulk sulfur isotope fractionations among bisulfite and other S (IV) compounds as a function of temperature, which appear to be highly dependent on the amount of $(HS)O_3^-$ present. Our new constraints on the bisulfite isomer quotient may allow for a detailed assessment of the molecular composition and isotope mass balance of S(IV) solutions containing HSO_3^-, and may be useful in the further investigation of the mechanisms and isotope fractionations associated with a number of processes that involve bisulfite compounds. These may include the intracellular enzymatic transformations of sulfite and bisulfite compounds that occur as part of dissimilatory sulfate reduction, which is a major and geologically important form of anaerobic respiration.

1. INTRODUCTION

Aqueous sulfite compounds (overall oxidation state: S^{4+}, or S(IV)) are produced and consumed by a variety of chemical and biological processes in natural environments

---

* Corresponding author.
  E-mail address: deldridge@carnegiescience.edu (D.L. Eldridge).

that span conditions from those of the atmosphere to the subseafloor biosphere. Sulfite compounds can be produced in the atmosphere by the hydrolysis of volcanogenic or anthropogenic $SO_{2(g)}$ emissions during the overall generation of acid rain and sulfate aerosols (e.g., Brandt and van Eldik, 1995). In low-temperature aqueous environments where aqueous sulfide (H_2S/HS^-) is continuously generated by anaerobic respiration (dissimilatory sulfate reduction), redox interfaces are often established based on opposing sulfide and oxygen concentration gradients where sulfite compounds can persist at relatively low concentrations due to their continuous production and consumption by chemical and biological oxidation processes (e.g., euxinic basins and organic-rich marine sediments: Millero, 1991; Zhang and Millero, 1993; Zopfi et al., 2001, 2004; Li et al., 2010). As part of this cycling, sulfite compounds can be additionally utilized by some microorganisms for sulfite compound disproportionation (e.g., Bak and Pfennig, 1987), an intriguing metabolism whose influence on global and environmental-scale sulfur cycling is still uncertain (Johnston, 2011). At the intracellular level, sulfite compounds are key intermediate substrates produced and consumed by enzyme-mediated reactions within microorganisms (bacteria and archaea) that carry out dissimilatory sulfate reduction (e.g., Ishimoto and Fujimoto, 1961; Peck, 1962; Kobayashi et al., 1974; Oliveira et al., 2008; Parey et al., 2010, 2013), and assimilatory sulfate reduction in bacteria, archaea, and plants that yields reduced sulfur for building principle amino acids (cysteine and methionine) and other functions (e.g., Canfield, 2001).

Of the many natural processes involving S(IV) compounds, dissimilatory sulfate reduction (DSR) is worthy of special consideration because it serves as a ubiquitous and influential pathway of anaerobic respiration that operates globally in organic-rich seafloor sediments (e.g., Jørgensen, 1982; Bowles et al., 2014), and has had a profound impact in the surficial geochemistry of the Earth throughout geologic history as inferred from the rock record (e.g., Canfield, 2001, 2004; Farquhar et al., 2010; Rickard, 2014). In addition to stimulating a global oxidative sulfur cycle (Jørgensen, 1977, 1982; Jørgensen et al., 1990; Canfield and Teske, 1996; Jørgensen and Nelson, 2004), aqueous sulfide (H_2S/HS^-) produced by DSR provides a primary source of reduced sulfur for authigenic pyrite (FeS_2) formation in marine sedimentary environments (e.g., Rickard, 2014). DSR has long been known to produce relatively large and variable sulfur isotope fractionations between extracellular sulfate and sulfide (e.g., Kaplan and Rittenberg, 1964; Sim et al., 2011a, 2011b; Leavitt et al., 2013, 2015) that can exert primary controls on the sulfur isotopic composition of geologically-preserved sulfur minerals such as authigenic pyrite and sulfate minerals, which in turn have been used to search for the earliest signs of the metabolism in the ancient rock record (e.g., Shen et al., 2001, 2009; Shen and Buick, 2004; Ueno et al., 2008; Wacey et al., 2011; see also Johnston, 2011). Such variability is generally understood to arise from factors that affect the overall expression of step-wise isotope fractionations associated with a series of intracellular enzyme-mediated reactions that centrally involve the production

and consumption of sulfite compounds (Parey et al., 2013; Wing and Halevy, 2014; Leavitt et al., 2015). Our understanding of the precise mechanisms and isotope effects associated with the enzyme-mediated transformation of sulfite compounds within sulfate reducing microorganisms will require a detailed understanding of the molecular composition of sulfite compounds in aqueous solution.

Sulfite compounds exhibit a complex speciation in aqueous solution that is often ignored in many models and considerations of the general DSR metabolism. This speciation alone may result in complex chemical and isotope fractionation behavior (Eldridge et al., 2016). A basic understanding of the molecular composition of S(IV) solutions is based on the relative stabilities of sulfite compounds via the following equilibrium reactions:

$$SO_{2(g)} \leftrightarrow SO_{2(aq)} \tag{1}$$

$$SO_{2(aq)} + H_2O \leftrightarrow HSO_3^- + H^+ \tag{2}$$

$$HSO_3^- \leftrightarrow SO_3^{2-} + H^+ \tag{3}$$

The relative distribution of S(IV) species therefore depends principally on the pH of the aqueous solution, and also on temperature and other variables such as ionic strength (μ). The equilibrium constants and other thermodynamic data (e.g., ΔH°_{rxn}) for these overall reactions are generally well-constrained (Goldberg and Parker, 1985; Millero et al., 1989). For example, at 25 °C and infinite dilution (low ionic strength), $SO_{2(aq)}$ dominates in solutions where pH < 1.9, HSO_3^- dominates over pH = 1.9–7.2, and SO_3^{2-} at pH > 7.2 ("dominates" means comprises ≥50% relative molar fraction). This indicates that HSO_3^- is an abundant if not dominant form of S(IV) over a wide range of solution conditions relevant to many natural systems including the intracellular environment of sulfate reducing organisms.

This simple picture is complicated by the more nuanced and somewhat uncertain molecular composition of bisulfite (HSO_3^-), which may be comprised of two distinct isomers (Golding, 1960; Connick et al., 1982; Horner and Connick, 1986; Littlejohn et al., 1992; Risberg et al., 2007). Bisulfite compounds can also undergo reactions with each other to form a dimer ($S_2O_5^{2-}$, $HS_2O_5^-$) when the overall HSO_3^- concentration is relatively high (Golding, 1960; Connick et al., 1982; Beyad et al., 2014). The two isomers of HSO_3^- differ in the structural site of protonation. One isomer contains a proton bound to an oxygen atom that can be represented as $(HO)SO_2^-$, and the other isomer contains a proton bound to the sulfur atom represented as $(HS)O_3^-$. An overall equilibrium for isomerization can be written as:

$$(HS)O_3^- \leftrightarrow (HO)SO_2^- \tag{4}$$

A corresponding equilibrium quotient (Q_i) can be written to represent their relative concentrations in solution ([] = concentration):

$$Q_i = \frac{[(HO)SO_2^-]}{[(HS)O_3^-]} \tag{5}$$

Experimental studies have investigated values for Q_i by means of ^{17}O-NMR, Raman, and sulfur K-edge XANES spectroscopies (Horner and Connick, 1986; Littlejohn

et al., 1992; Risberg et al., 2007). However, these studies were carried out with solution compositions that are not always comparable, in particular whether additional components were added to increase the total ionic strength. The three studies generally agree in that $Q_i > 1$ (i.e., the HO-isomer is more abundant and therefore more stable) and that Q_i decreases with increasing temperature (i.e., the HS-isomer increases in relative molar proportion with increasing temperature). Existing data do not seem to converge on similar values for Q_i under otherwise comparable conditions. For example, Q_i may range somewhere between ~2.7 to 5 at 25 °C with an uncertain dependence on ionic strength (Horner and Connick, 1986; Littlejohn et al., 1992; Risberg et al., 2007). It is not clear whether these differences arise from differences in solution composition between the studies, or from the spectroscopic approach employed and the accompanying assumptions taken to estimate the quotient from the different spectroscopic methods used (or some combination thereof). Theoretical investigations may be able to shed light onto the relative stabilities of the two isomers, but so far have not yielded quantitatively reliable results (Steudel and Steudel, 2009).

We provide new experimental estimates for the bisulfite isomer quotient (Eq. (5)) *via* the interpretation of Raman spectra collected from aqueous bisulfite solutions over 5–85 °C and [NaHSO₃] = 0.2–0.4 m (moles per kg H₂O) up to a total ionic strength of $\mu = 1.0$ m (NaHSO₃ + NaCl). These new estimates of Q_i are employed to re-assess sulfur isotope fractionations in aqueous S(IV) systems, following and incorporating the results of recent theoretical calculations of equilibrium sulfur isotope fractionations among S(IV) compounds (Eldridge et al., 2016). The combination of Raman estimates of Q_i and the compound specific theoretical sulfur isotope fractionation factors of Eldridge et al. (2016) may allow for an assessment of the isotopic mass balance of S(IV) solutions over a wider range of conditions than have previously been available. These constraints may aid in the interpretation of sulfur isotope fractionations associated with a number of processes that involve bisulfite compounds. For example, these constraints may be useful in the further investigation of the mechanisms and isotopic fractionations associated with the intracellular enzymatic transformations of sulfite compounds that occurs as part of dissimilatory sulfate reduction, a major and geologically important form of anaerobic respiration.

2. METHODS

2.1. Overview

The majority of the experiments were performed with aqueous solutions of sodium bisulfite (NaHSO₃) contained in fused silica capsules (FSCs), which facilitated the collection of Raman spectra as a function of temperature. Additional experiments were performed in a custom built sapphire window cell at room temperature to test hypotheses regarding the interpretation of our spectra (discussed in Sections 3.2 and 4.2). Three types of experiments were performed: (1) experiments run from 85 °C to 5 °C (descending temperature) in FSCs loaded with aqueous bisulfite solu-

tions of different concentration ([NaHSO₃] = 0.2, 0.3, and 0.4 m), and another with added NaCl to increase ionic strength ([NaHSO₃] = 0.2 m, [NaCl] = 0.8 m; $\mu = 1.0$ m), (2) time-series experiment conducted at 65, 25, and 5 °C in an FSC in order of descending temperature ([NaHSO₃] = 0.3 m), and (3) three room-temperature experiments where aqueous bisulfite solutions were contained within a custom built sapphire window cell ([NaHSO₃] = 0.3 m) prepared at different pH values (pH = 4.4, 3.8, and 3.3). A summary of the experiments can be found in Table 1.

2.2. Bisulfite solutions

Aqueous solutions of 0.2, 0.3, and 0.4 m NaHSO₃ (mol/kg) were prepared from Na₂S₂O₅ salts (≥99%, Sigma Aldrich) and N₂-purged deionized water (Alfa Aesar). Solutions were prepared in a vinyl anaerobic chamber containing a 95:5% N₂:H₂ atmosphere circulated through palladium catalyst boxes (Coy Laboratory Products). Measurements of pH were performed on aliquots of stock sodium bisulfite solutions at room temperature in the anaerobic chamber by using a gel filled combination electrode (Thermo Scientific) calibrated via standard buffers. Solutions were prepared without pH adjustment, with the exception of the two experiments performed in the sapphire window cell at pH values of 3.8 and 3.3 with the pH adjusted with small amounts of 2.5 M HCl. For the one experiment performed with ionic strength as the additional variable (0.2 m NaHSO₃), the solutions were prepared as above with the addition of NaCl (≥99.9% Enzyme Grade, FisherBiotech) to bring the total ionic strength of the solution to 1.0 m (i.e., 0.8 m NaCl).

2.3. Fused silica capsules (FSCs)

The fused silica capsules were prepared from round silica tubes with dimensions of 1.0 mm O.D. × 0.5 mm I.D. (National Scientific Company, Quakertown, PA). These were cut into lengths of approximately 17–18 mm and sealed on one end using an C₂H₂/O₂ torch. Approximately 1–1.2 μL of freshly prepared NaHSO₃ solution was loaded into the sealed end of a fused silica tube using a 10 μL syringe with 32-gauge needle (0.24 mm O.D.; Hamilton Company) in the anaerobic chamber. Tubes containing NaHSO₃ solutions were then immediately frozen in liquid nitrogen in the anaerobic chamber, and kept frozen until sealed by C₂H₂/O₂ torch in the ambient atmosphere in order to avoid contamination of the fluid by air that could change solution composition via the oxidation of bisulfite (i.e., sulfate production and a decrease in pH). During the torch sealing in the ambient atmosphere, tubes containing sodium bisulfite were kept frozen by their containment in an insulating silver tube emerged in liquid nitrogen. Additionally, a low flow of ultrapure argon gas (Roberts Oxygen Supply) over the frozen tube was used to displace air in the tube headspace immediately prior to sealing to further minimize air contamination. The lack of a detectable band at ~980 cm⁻¹ in Raman spectra, which could correspond to the characteristic S-O symmetric stretch of the aqueous SO₄²⁻ ion, was taken as evidence that the NaHSO₃ solutions

Table 1
Summary of experiments and conditions. FSC = Fused Silica Capsule, SWC = Sapphire Window Cell.

Experiment	T (°C)	[NaHSO$_3$] (m)	pH[a]	Capsule
5–85 °C	85, 65, 45, 25, 15, 5	0.20	4.5	FSC
5–85 °C	85, 65, 45, 25, 15, 5	0.20 (+0.80 m NaCl)[b]	N/A[b]	FSC
5–85 °C	85, 65, 45, 25, 15, 5	0.30	4.4	FSC
5–85 °C	85, 65, 45, 25, 15, 5	0.40	4.4	FSC
Time series	65, 25, 5	0.30	4.5	FSC
Sapphire Window	∼25 (room)	0.30	4.4	SWC
Sapphire Window	∼25 (room)	0.30	3.8	SWC
Sapphire Window	∼25 (room)	0.30	3.3	SWC

[a] Room temperature pH measurements.
[b] Total ionic strength: μ = 1.0 m (pH not determined).

had not undergone any detectable oxidation during the sealing process. The resulting FSCs were typically 17–18 mm in length with the meniscus of our NaHSO$_3$ solution positioned at or near the center of the capsule (see supplementary material to view an image of a representative FSC).

2.4. Temperature stage

Raman spectra of NaHSO$_3$ solutions in FSCs were collected as a function of temperature over 85–5 °C using a Linkam THMS600 heating and freezing microscope stage (thermal stability ∼0.01 °C; Linkam Scientific Instruments, U.K.). Single FSCs were secured to the sample heating/-cooling portion of the stage that measures ∼24.5 mm in diameter using thermal Teflon tape with the meniscus positioned near the center of the stage to enable fluid and glass background measurements for background subtraction procedures. The FSCs were crafted to fit completely on the sample heating/cooling stage without any overhang, and were typically ∼2–3 mm from the outer edge of the sample heating/cooling area. Negligible thermal gradients from the center to the outer edge of the sample heating/-cooling stage were observed (i.e., within the ≤1 °C precision of measurements using a 0.003 mm diameter Chromega-Alomega K-type thermocouple; OMEGA Engineering, Inc.). Experimental runs were conducted in descending temperature from 85 °C to 45 °C in 20 °C intervals utilizing the T95-HS heating stage controller, and from 25 °C to 5 °C in 10 °C intervals using the LNP95 cooling pump chilled via liquid nitrogen Dewar attachment (Linkam Scientific Instruments, U.K.). Time series experiments ([NaHSO$_3$] = 0.3 m) at 65 °C, 25 °C, and 5 °C were performed over ∼3 h intervals per temperature, and also run in order of descending temperature using the same respective temperature controller configurations.

2.5. Sapphire cell

Several experiments were performed with a custom-built sapphire-window cell for the collection of Raman spectra from bisulfite solutions (0.3 m NaHSO$_3$) under room temperature conditions (∼25 °C) to test hypotheses regarding the interpretation of our spectra (discussed in Sections 3.2

and 4.2). The cell was crafted from the upper screw-top half of a ∼1.5 ml septa vial (borosilicate glass; Waters Corporation) adhered to a sapphire window (12.0 mm diameter, 1.0 mm thickness; Guild Optical Associates), which served as the optical window for the Raman measurements. For the preparation of the cell, the borosilicate vial was cut in half with the cut surface ground flat and polished prior to the adhesion of the sapphire window using Crystalbond™ resin (acetone-soluble). Bisulfite solutions (0.3 m NaHSO$_3$) were prepared exactly as above in the anaerobic chamber, loaded into the cell without headspace using a graduated pipette, and sealed using the stock PTFE/Silicone screw-top septa cap while under anoxic conditions. Raman measurements were performed immediately after the cell was loaded with bisulfite solution and removed from the anaerobic chamber.

2.6. Raman measurements

Raman spectra were obtained with a JASCO NRS-3100 Laser Raman Spectrophotometer using 490 nm (blue) laser excitation. Acquisitions were performed using an Olympus 50× objective, 1200 lines/mm grating, and entrance slit of 0.05 mm (resolution ∼4 cm^{-1}). The typical laser power reaching samples was on the order of 35–40 mW. No resolvable difference in Raman spectra or the quantitation of bands was observed with increasing laser power over a range of ∼3–40 mW, which indicates that the laser power utilized did not induce reactions with the bisulfite compounds. For the 5–85 °C experiments, spectra were recorded over the range of 330–4290 cm^{-1} split into three spectral windows with 300-s acquisition times acquired in duplicate for each window. For the time series and sapphire window experiments, spectra were collected in an identical manner but typically only in a single spectral window over the range of ∼330–2500 cm^{-1}. Raman spectra collected from fluid contained in FSCs were background corrected by subtracting the identically collected glass/headspace spectra at a given temperature (i.e., identical settings, orientation, and optical depth). Similarly, spectra collected from the sapphire window cell were background-corrected by subtracting the spectra of the empty cell collected under the same acquisition settings and optical depth. Following background subtraction, the spectra were linearly baseline corrected and curve-fitted with pseudo-Voigt functions to

determine Raman peak positions and integrated intensities (i.e., peak area, A) for assignment and quantification purposes.

2.7. Estimation of the bisulfite isomer quotient (Q_i)

The concentration ratio of the two bisulfite isomers at a given temperature and bisulfite concentration is estimated from the ratio of the integrated intensities (A) of two overlapping bands in the Raman spectrum centered at approximately 1020 and 1050 cm^{-1} attributable to the symmetric S-O stretching vibrations of each isomer (Connick et al., 1982 and references therein; Littlejohn et al., 1992; Risberg et al., 2007):

$$Q_i = \frac{[(HO)SO_2^-]}{[(HS)O_3^-]} \approx \frac{A_{v(s)(S-O)(HO\ isomer)}}{A_{v(s)(S-O)(HS\ isomer)}} = \frac{A_{1020}}{A_{1050}} \qquad (6)$$

The integrated intensities (or "peak areas", A) were determined from the spectra by way of multi peak curve fitting procedures. The subscripts "$v(s)$ (S-O)" indicate that the intensities correspond to the symmetric stretching vibrations (v_s) of the sulfur-oxygen bonds (S-O) in each isomer (we will show that the $\sim$1020 cm^{-1} and $\sim$1050 cm^{-1} bands correspond to the $(HO)SO_2^-$ and $(HS)O_3^-$ isomers, respectively; cf. Littlejohn et al., 1992). For this approximation of the concentration ratio, we must assume similar Raman cross sections for the analogous S-O symmetric stretching vibrations associated with the two isomers.

Our determination of this integrated intensity ratio was complicated by the observation of a shoulder on the high frequency side of the $\sim$1050 cm^{-1} band that appears to arise from an additional Raman feature in this region of the spectrum. A protocol was developed and undertaken to both (1) estimate the position and dimensions of the unresolved feature, and (2) estimate $A_{v(s)(S-O)(HO\ isomer)}/A_{v(s)(S-O)(HS\ isomer)}$ for each spectrum taking into consideration the uncertain position/dimensions of the unresolved feature. The details of these procedures are discussed in Section 3.2.

3. RESULTS

3.1. Raman spectra of aqueous NaHSO$_3$ solutions in FSCs: general features

Representative Raman spectra collected as a function of temperature by using the FSCs are shown in Figs. 1 and 2 over different spectral ranges ([NaHSO$_3$] = 0.3 m is shown). The strong overlapping bands centered at $\sim$1020 cm^{-1} and $\sim$1050 cm^{-1} can be attributed to the symmetric stretching vibrations (v_s) associated with the sulfur-oxygen bonds from each of the two bisulfite isomers (Connick et al., 1982 and references therein; Littlejohn et al., 1992; Risberg et al., 2007; specific assignments to $(HS)O_3^-$ and $(HO)SO_2^-$ are discussed in Section 3.3). The relative intensities of these two bands vary with temperature (Figs. 1 and 2), in qualitative agreement with previous studies (Littlejohn et al., 1992). The $\sim$2520 cm^{-1} band results from an H-S stretching vibrational frequency (v) and may be considered diagnostic of the $(HS)O_3^-$ isomer (Connick et al.,

1982 and references therein). Much weaker bands can be seen at $\sim$585 cm^{-1} and $\sim$1120 cm^{-1} and have been previously attributed to a bending modes (δ) associated with $(HO)SO_2^-$ and $(HS)O_3^-$, respectively (Meyer et al., 1979; Connick et al., 1982; Risberg et al., 2007). The $\sim$1620 and $\sim$3200–3600 cm^{-1} bands (latter not shown) are all characteristic of H-O and H-O-H vibrations (e.g., Frantz et al., 1993). The lower intensity $\sim$1620 cm^{-1} band corresponds to the characteristic H-O-H bending mode (δ), and the suite of overlapping higher frequency bands correspond to H-O stretching vibrational modes (maximum at ca. 3400 cm^{-1} with a $\sim$3620 cm^{-1} shoulder) and a lower frequency shoulder feature interpreted to result from intermolecular hydrogen bonding ($\sim$3250 cm^{-1}; e.g., Frantz et al., 1993). An H-O stretching frequency resulting from the $(HO)SO_2^-$ isomer is expected to be observed in the high frequency water range (ca. 3150 cm^{-1}; Risberg et al., 2007), but it is heavily overprinted by the much higher intensity bands assigned to vibrations of H$_2$O. Any other bands that previous workers have observed and attributed to either of the bisulfite isomers (e.g., at ca. 467, 506, and 730 cm^{-1}; Connick et al., 1982) appear to be too weak to be easily resolved in our spectra.

The possibility exists that the bisulfite dimer ($S_2O_5^{2-}$) may contribute to the observed $\sim$1050 cm^{-1} band due to its having a similar S-O stretching vibrational frequency (ca. 1052 cm^{-1} at 25 °C; Connick et al., 1982 and references therein). By using the recent determination of the dimerization quotient at 25 °C in low ionic strength media (Q_d = 0.045 M^{-1}; Beyad et al., 2014), we estimate a dimer concentration on the order of [$S_2O_5^{2-}$] $\sim$ 0.002–0.007 m in our solutions of [NaHSO$_3$] = 0.2–0.4 m (assuming negligible differences between molarity and molality). From previous Raman studies, other bands associated with $S_2O_5^{2-}$ may be expected within our measured spectral range at ca. 425, 556, 655, 966, and 1170 cm^{-1} (Herlinger and Long, 1969; Connick et al., 1982 and references therein). Of these, the $\sim$425 and 655 cm^{-1} bands are expected to be the strongest (Herlinger and Long, 1969), and from the analysis of Littlejohn et al. (1992) the $\sim$655 cm^{-1} band may yield a comparable intensity with concentration as the $\sim$1020 and $\sim$1050 cm^{-1} bands. None of these bands were observed in Raman spectra collected from [NaHSO$_3$] = 0.2–0.4 m, which in combination with the expected low relative concentration of $S_2O_5^{2-}$ may indicate that the dimer does not contribute significantly to the spectra. It is tentatively concluded, therefore, that dimers may not contribute significantly to the intensity of the observed $\sim$1050 cm^{-1} band. We assume negligible contributions from the dimer throughout this study, but will return to this question in subsequent sections (Section 3.4) when we compare the integrated intensity ratios of the $\sim$1020 and $\sim$1050 cm^{-1} bands at different concentrations of NaHSO$_3$.

There is no evidence for aqueous sulfur dioxide (SO$_{2(aq)}$; $v_{s\ (S-O)} \sim$ 1150 cm^{-1}) or the sulfite ion (SO$_3^{2-}$; $v_{s\ (S-O)} \sim$ 967 cm^{-1}) in any of the bisulfite solutions having room temperature pH = 4.4–4.5 (Fig. 2). This is consistent with their very low expected concentrations under these conditions (i.e., SO$_{2(aq)} \sim$ 0.2–0.3% and SO$_3^{2-} \sim$ 0.2% of total S(IV); Goldberg and Parker, 1985; Millero et al., 1989). We do
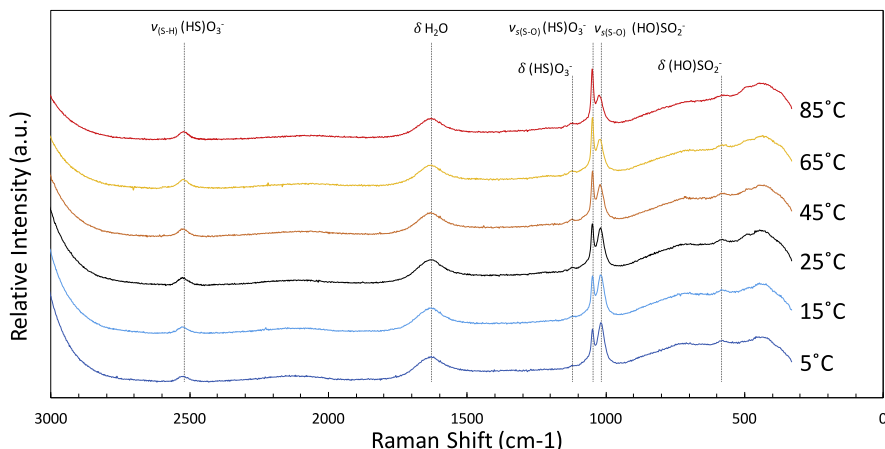
Fig. 1. Raman spectra collected from a representative aqueous $NaHSO_3$ solution (0.3 m $NaHSO_3$) contained in a fused silica capsule over 5–85 °C (background subtracted). Vertical lines denote bands and their assignments: $v_{s(S-O)}$ indicate symmetric stretching bands for sulfur-oxygen bonds, $v_{(S-H)}$ indicates a sulfur-hydrogen stretching band, and δ indicate bending modes.
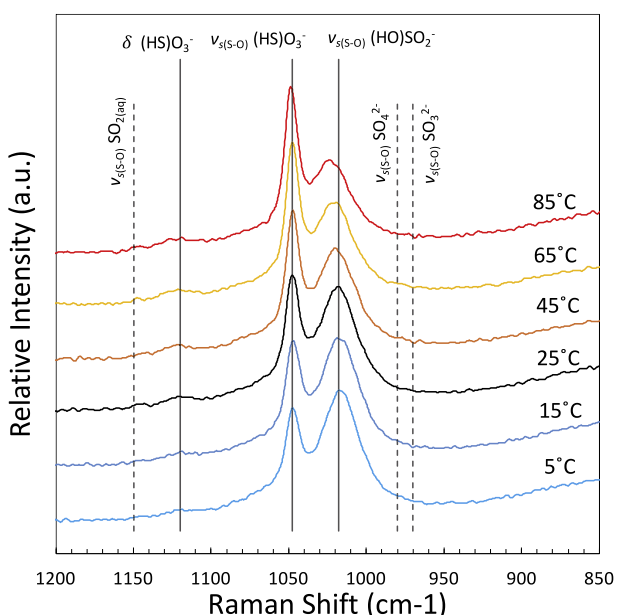

Fig. 2. Raman spectra collected from an aqueous 0.3 m $NaHSO_3$ solution contained in a fused silica capsule over 5–85 °C as in Fig. 1 with special focus on the sulfur-oxygen stretching region. Vertical lines indicating bands and assignments are labeled as in Fig. 1. Dashed vertical lines indicate the approximate Raman shifts for v_s $_{(S-O)}$ bands of other aqueous S(IV) compounds ($SO_{2(aq)}$, SO_3^{2-}) and sulfate (SO_4^{2-}), and are included for reference.

resolve the ~1150 cm^{-1} band in room temperature experiments performed in the sapphire window cell with the pH adjusted to lower values (3.8 and 3.3) and where increased amounts of $SO_{2(aq)}$ are expected.

There is no evidence for the sulfate ion (SO_4^{2-}; v_s $_{(S-O)}$ ~ 980 cm^{-1}) that could be present in the solutions either as a blank from the precursor $Na_2S_2O_5$ salts or as a bisulfite oxidation product. The bisulfate ion (HSO_4^-) exhibits a Raman band corresponding to an S-O symmetric stretching vibration in close proximity to the analogous bands for the bisul-

fite compounds (v_s $_{(S-O)}$ ~ 1052 cm^{-1}; e.g., Rudolph, 1996). The equilibrium constant (K) for the dissociation reaction of HSO_4^- ($HSO_4^- = SO_4^{2-} + H^+$) is in close proximity to a value of $-\log K \sim 2$ over the temperature range we have studied and under comparable total ionic strength (e.g., Rudolph, 1996; see also Supplementary Material). Thus, the SO_4^{2-} ion is expected to be in greater abundance than the HSO_4^- ion by orders of magnitude under the conditions of our solutions. The lack of evidence for SO_4^{2-} therefore precludes any interference in our spectra resulting from the HSO_4^- ion, and overall is taken to indicate that our bisulfite compounds did not undergo detectable oxidation during solution preparation or the torch sealing of FSCs.

3.2. Integrated intensities of Raman bands from curve fitting procedures

Our quantification of A for each of the three clear overlapping bands in the 1000–1200 cm^{-1} region (i.e., A_{1020}, A_{1050}, and A_{1120}) is complicated by the observation of a shoulder on the high frequency side of the ~1050 cm^{-1} band that appears to arise from an additional feature in this region of the spectrum[1]. A representative example of curve fitting results to one of our spectra (Fig. 3) illustrates this feature. A band from the silica glass background exists in this region around ~1050–1055 cm^{-1} (e.g., Seifert et al., 1983; Phillips, 1984), but it does not seem that such a feature is the primary contributor to this shoulder because: (1) the minimization of the silica background via careful choice of focal depth of the laser into the fluid does not affect the intensity, (2) the procedure of subtracting the glass background from our spectra would have eliminated this feature, and (3) we observe the same shoulder feature in spectra collected from solutions in the sapphire window cell (Al_2O_3), which does not contain possible background

---

[1] In principle, this shoulder may be the expression of more than one unresolved band, but for the purposes of the present study we will take the parsimonious route and assume it is a singular band.
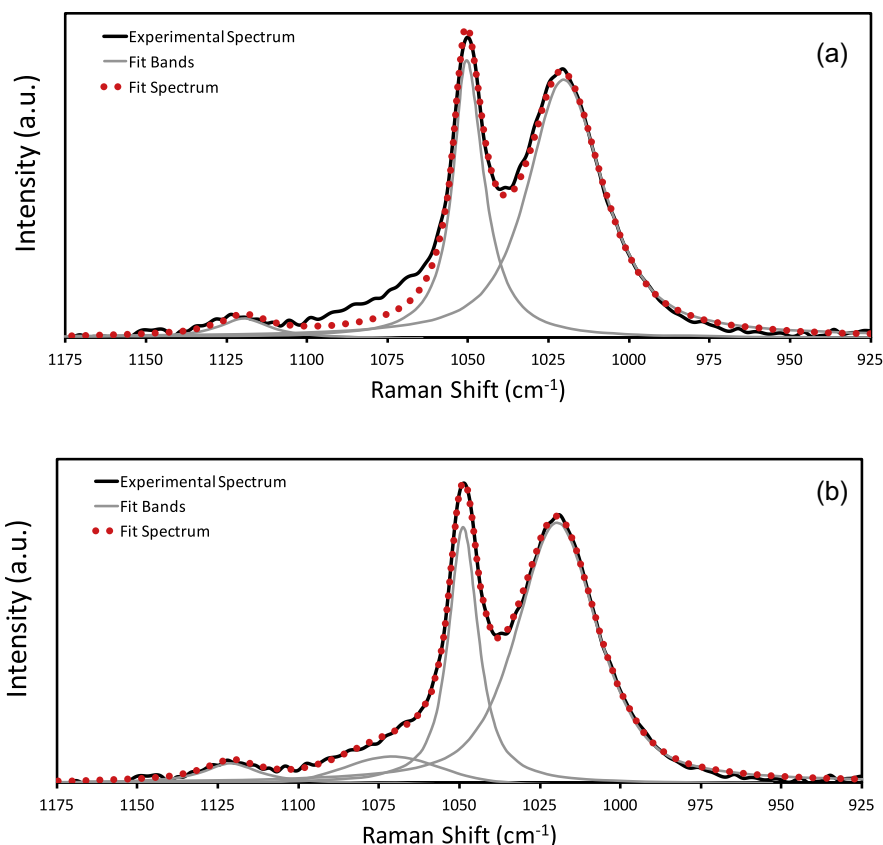
Fig. 3. (a-b): Example results of our multi-peak fitting exercise for quantifying the integrated intensities of Raman bands (i.e., peak areas; A) in the sulfur-oxygen stretching region (0.3 m NaHSO$_3$ in a FSC at 25 °C). Figure (a) indicates a peak fitting exercise assuming only the three obvious bands, where a clear misfit occurs between the ~1050 cm^{-1} and ~1120 cm^{-1} bands. The misfit is due to a relatively high shoulder on the high frequency side of the ~1050 cm^{-1} band that appears to arise from an additional band. Figure (b) indicates a similar exercise but with the inclusion of a fourth band that was deemed necessary to include to obtain more accurate estimations of A_{1020}, A_{1050}, and A_{1020}/A_{1050}.

Raman bands in this region. Thus, the feature responsible for the shoulder on the high frequency side of the ~1050 cm^{-1} band appears to arise from the aqueous solution. For the purposes of the present study, this unresolved band can be viewed as an interference that introduces uncertainty into our determination of A_{1020}, A_{1050}, A_{1120}, and most importantly the A/A ratio of the ~1020 and ~1050 cm^{-1} bands (A_{1020}/A_{1050}).

In an attempt to account for the unresolved feature in our area determination for proximal bands, a protocol was developed that allowed us to estimate A_{1020}, A_{1050}, A_{1120}, and A_{1020}/A_{1050} while taking into consideration the uncertain position and dimensions of the interfering band. The procedure is to first estimate the positions and FWHM (full width at half maximum) for the ~1020, ~1050, and ~1120 cm^{-1} bands by inspection for each spectrum. The FWHM parameters were then used as fixed constraints in curve fitting procedures to estimate the position and FWHM of the unresolved shoulder feature in each of the spectra. This analysis yields a mean position of 1068 ± 3 cm^{-1} (median ~1069 cm^{-1}) and a mean FWHM of 39 ± 5 cm^{-1} (median ~40 cm^{-1}) for the poorly resolved band from 18 spectra collected over 5–85 °C and [HSO$_3^-$] = 0.2–0.4 m in FSCs. A series of curve fits for each spectrum was then performed where we fixed the unresolved feature

to positions ranging 1065–1075 cm^{-1} and FWHM ranging 35–45 cm^{-1} (in 5 cm^{-1} intervals each) while relaxing constraints on the ~1020, ~1050, and ~1120 cm^{-1} bands. This procedure yields 9 fits and values of A_{1020}, A_{1050}, A_{1120}, and A_{1020}/A_{1050} for each spectrum based on 9 unique imposed position/FWHM combinations for the unresolved feature. The mean of these nine values of each of these quantities was taken to obtain our estimate of A_{1020}, A_{1050}, A_{1120}, and A_{1020}/A_{1050} for a given spectrum (Table 2). The standard deviation of these mean values is interpreted to be the associated error in A_{1020}, A_{1050}, A_{1120}, and A_{1020}/A_{1050} because of the uncertain dimensions of the unresolved feature. Similar fit results from the time series and sapphire window cell experiments can be found in Tables 3 and 4, respectively, where the fits to spectra collected at lower pH values (3.3 & 3.8) in the sapphire window cell include an additional band corresponding to SO$_{2(aq)}$ at ~1150 cm^{-1}.

3.3. Assignment of the 1020 and 1050 cm^{-1} Raman Bands to (HO)SO$_2^-$ and (HS)O$_3^-$

The assignment of the two strong overlapping Raman bands in the frequency range of the S-O stretch vibrations centered at ca. 1020 and 1050 cm^{-1} has been made to each

Table 2
Summary of results from peak fitting procedures for bands from 5 to 85 °C experiments in fused silica capsules. Raman Shifts and FWHM are in units of cm^{-1}.

[NaHSO$_3$] (m)	T (°C)	Raman Shift	FWHM	A_{1020}	±	Raman Shift	FWHM	A_{1050}	±	Raman Shift	FWHM	A_{1120}	±	Raman Shift	FWHM	A_{2520}	A_{1020}/A_{1050}	±
0.20	85	1022	31	43,511	1632	1047	10	25,943	1221	1120	25	3490	909	2520	46	21492	1.68	0.11
	65	1020	30	47,810	1098	1047	10	26,256	2239	1119	30	4512	803	2521	45	14035	1.83	0.19
	45	1018	30	44,479	786	1046	10	24,254	833	1120	17	2145	576	2522	45	13917	1.84	0.09
	25	1017	30	46,706	1025	1046	11	19,169	1776	1117	31	2284	721	2523	41	7850	2.46	0.25
	15	1016	30	47,625	1029	1046	11	15,304	2707	1121	21	1609	820	2524	38	6839	3.20	0.58
	5	1016	29	50,084	1101	1047	12	18,581	1700	1118	30	2467	733	2524	43	5823	2.72	0.31
0.30	85	1023	31	73,358	1200	1049	10	42,647	1259	1122	33	10920	737	2522	43	29774	1.72	0.07
	65	1021	30	84,576	1794	1048	10	41,729	2267	1122	32	13115	1707	2522	43	24972	2.03	0.12
	45	1019	30	88,769	847	1047	10	38,940	1409	1122	28	10571	549	2523	42	19708	2.28	0.10
	25	1018	30	96,937	1491	1048	11	37,975	2302	1120	26	9044	1713	2524	44	17396	2.56	0.18
	15	1017	30	99,390	1254	1047	12	34,846	1737	1120	31	8582	1313	2524	43	15552	2.86	0.17
	5	1017	29	103,368	1354	1047	11	31,418	2483	1119	28	6187	1603	2523	44	12450	3.31	0.29
0.40	85	1022	31	110,874	2277	1048	10	64,036	1904	1122	29	15645	1892	2521	44	54031	1.73	0.07
	65	1021	31	114,820	2622	1048	10	60,173	1920	1123	25	14563	1968	2522	45	45255	1.91	0.08
	45	1019	31	121,993	1477	1048	11	57,517	1244	1121	30	15277	1363	2523	42	34796	2.12	0.06
	25	1018	29	136,731	2158	1047	11	49,533	3624	1121	25	9380	1854	2525	-	-	2.78	0.24
	15	1017	30	142,919	1437	1047	11	46,632	3377	1119	28	9762	1705	2525	-	-	3.08	0.25
	5	1017	30	140,501	1350	1048	12	41,013	2529	1120	25	4735	1049	2526	35	18405	3.44	0.25
0.20 (+ 0.80 m NaCl)	85	1025	33	29,552	875	1049	10	17,321	1148	1121	37	3534	326	2521	43	15781	1.71	0.14
	65	1022	30	31,060	827	1048	10	17,609	747	1123	30	3059	407	2524	49	12814	1.77	0.11
	45	1020	30	31,075	855	1048	10	16,769	895	1121	33	2177	539	2524	46	10116	1.86	0.14
	25	1019	30	35,646	1194	1048	11	14,511	844	1122	22	1452	650	2524	45	8881	2.47	0.21
	15	1019	30	37,642	1471	1048	11	12,022	1601	1120	29	2010	570	2525	47	5915	3.18	0.46
	5	1018	29	38,789	837	1048	12	13,750	2630	1114	27	1711	357	2527	41	4731	2.93	0.64

Table 3

Summary of results of peak fitting procedures from the time series experiment prepared at 0.30 m NaHSO$_3$. Raman Shifts are in units of cm^{-1}.

T (°C)	Time (h)	Raman Shift	A_{1020}	±	Raman Shift	A_{1050}	±	Raman Shift	A_{1120}	±	A_{1020}/A_{1050}	±
65	0.00	1021	86,840	1233	1048	49,843	2364	1121	9153	705	1.75	0.10
65	0.17	1021	92,287	2345	1048	48,851	2205	1121	7860	698	1.89	0.13
65	0.35	1021	91,359	1527	1047	48,740	1931	1121	10,489	1417	1.88	0.07
65	0.52	1021	89,389	2170	1048	48,560	2116	1119	7390	1126	1.85	0.12
65	0.68	1021	91,676	1230	1047	48,310	1801	1120	7991	897	1.90	0.08
65	0.87	1021	89,570	1885	1048	48,633	1765	1120	7452	1116	1.84	0.09
65	1.03	1021	90,097	1422	1048	47,414	1642	1121	9824	1211	1.90	0.08
65	1.45	1021	92,130	1498	1048	51,054	2980	1121	10,212	981	1.81	0.13
65	1.97	1021	93,554	1452	1048	51,533	2907	1120	10,688	1288	1.82	0.12
65	2.40	1021	89,101	1499	1048	49,782	2501	1122	8904	928	1.79	0.12
65	2.82	1021	91,862	1503	1047	48,194	2507	1121	8101	1136	1.91	0.10
25	0.00	1018	104,646	1498	1048	38,009	2046	1122	4498	1344	2.76	0.18
25	0.18	1019	104,293	2091	1048	34,873	1817	1123	3505	1388	3.00	0.19
25	0.35	1018	105,606	1618	1048	36,253	1842	1121	3505	1388	2.92	0.16
25	0.52	1019	103,622	1306	1048	39,225	2147	1122	3842	1097	2.65	0.17
25	0.70	1019	104,985	1224	1048	37,376	2169	1122	5896	1172	2.82	0.19
25	0.87	1019	105,241	1864	1048	36,518	1370	1121	6025	1961	2.89	0.11
25	1.03	1019	106,040	1941	1048	37,434	1907	1123	2865	752	2.84	0.18
25	1.50	1018	102,461	1436	1048	39,167	1836	1122	4491	1289	2.62	0.14
25	2.03	1019	103,470	1575	1048	36,667	1897	1121	4962	1382	2.83	0.16
25	2.45	1019	102,846	1609	1048	38,541	1532	1121	4570	1618	2.67	0.13
25	2.87	1019	100,820	1836	1048	38,077	2137	1123	3224	1169	2.66	0.18
5	0.00	1018	106,478	1562	1049	33,696	3444	1120	4502	921	3.19	0.39
5	0.17	1017	105,975	1208	1048	33,225	2529	1120	3522	1076	3.21	0.28
5	0.52	1017	106,775	1476	1048	33,885	2670	1120	2881	1062	3.17	0.31
5	0.68	1018	109,858	1091	1049	32,120	3177	1121	3719	789	3.45	0.39
5	0.85	1017	108,089	1434	1048	34,016	3190	1120	5278	1300	3.21	0.36
5	1.03	1017	108,746	1308	1048	30,383	3298	1120	4042	815	3.62	0.45
5	1.53	1017	105,899	1474	1048	32,492	3578	1121	3736	1372	3.30	0.42
5	2.00	1017	110,879	1120	1048	30,448	3188	1120	4067	972	3.68	0.41
5	2.42	1017	108,938	1183	1048	33,374	3549	1121	3353	912	3.30	0.39
5	2.83	1017	108,503	1721	1048	35,398	2792	1122	2657	604	3.09	0.32

of the two bisulfite isomers *via* the comparison of their integrated intensities to those of the ~2520 cm^{-1} band as a function of temperature. The ~2520 cm^{-1} band unambiguously corresponds to the H-S stretching vibrational frequency of the (HS)O$_3^-$ isomer (Connick et al., 1982 and references therein). The relative concentration of the bisulfite isomers varies with temperature, and so the comparison of A_{1020} and A_{1050} to A_{2520} over a temperature range should allow for relatively straightforward assignment of the ~1020 and ~1050 cm^{-1} bands to either of the bisulfite isomers. This procedure does not require any assumption regarding which isomer is in greater abundance at any given temperature, or rely on any assumption about which isomer's relative abundance increases/decreases with temperature. The A_{1020} and A_{1050} vs. A_{2520} collected from the 5–85 °C experiments indicate that the 1050 cm^{-1} band positively correlates with the 2520 cm^{-1} band while the 1020 cm^{-1} band correlates negatively with the 2520 cm^{-1} band for each bisulfite concentration (Table 2), clearly indicating that the ~1050 cm^{-1} band corresponds to (HS)O$_3^-$ isomer and the ~1020 cm^{-1} band to the (HO)SO$_2^-$ isomer. This is the same assignment made by Littlejohn et al. (1992) following similar reasoning. A similar exercise with the ~1120 cm^{-1} band at the end member temperatures of 5 and 85 °C (Table 2) might corroborate earlier worker's assignments of

this band to the (HS)O$_3^-$ isomer (Meyer et al., 1979; Connick et al., 1982), but the features of the ~1120 cm^{-1} band are perhaps too poorly resolved to allow for much quantitative analysis.

3.4. Values of A_{1020}/A_{1050} as a function of time, bisulfite concentration, and temperature

The results from the time series experiment performed at 0.3 m NaHSO$_3$ are presented in Fig. 4a, which displays ln(A_{1020}/A_{1050}) at 65 °C, 25 °C, and 5 °C, from spectra collected over 3 h intervals at each temperature. There are no clear trends towards higher or lower values of A_{1020}/A_{1050} as a function of time at any given temperature with mean and standard deviation of the mean for values of A_{1020}/A_{1050} at 1.85 ± 0.05 at 65 °C, 2.79 ± 0.12 at 25 °C, and 3.32 ± 0.20 at 5 °C (i.e., relative standard deviation ± 4–5%). These mean values (as natural logarithms) are plotted as horizontal lines in Fig. 4a.

The ln(A_{1020}/A_{1050}) as a function of temperature (1/T) for each of the different concentrations of bisulfite ([NaHSO$_3$] = 0.2, 0.3, and 0.4 m) are shown in Fig. 4b-d. Each experiment performed at a different bisulfite concentration yields comparable trends in ln(A_{1020}/A_{1050}) with temperature. The least squares linear regression of each 6-

Table 4
Results of peak fitting procedures for experiments performed in the sapphire window cell at room temperature and 0.30 m NaHSO$_3$. Raman Shifts and FWHM are in units of cm^{-1}.

pH	Raman Shift	FWHM	A_{1020}	±	Raman Shift	FWHM	A_{1050}	±	Raman Shift	FWHM	A_{1120}	±	Raman Shift	FWHM	A_{1150}	±	A_{1020}/A_{1050}	±
4.4	1016	30	285,658	1502	1045	11	103,109	5084	1118	27	31,392	1532	N/A	N/A	N/A	N/A	2.78	0.15
3.8	1021	29	134,354	2320	1051	11	49,897	962	1125	15	5411	305	1150	8	2552	65	2.69	0.06
3.3	1020	30	155,030	4072	1050	11	49,025	2346	1123	33	17,524	2018	1149	7	7546	353	3.17	0.12

point dataset collected over 5–85 °C (filled black circles in Fig. 4b-d) yields:

$$\ln(A_{1020}/A_{1050}) = 753(\pm166)/T - 1.63(\pm0.53) \quad \text{at} \quad 0.2 \text{ m}$$
NaHSO$_3$ (r^2 = 0.84),
$$\ln(A_{1020}/A_{1050}) = 755(\pm45)/T - 1.55(\pm0.15) \quad \text{at} \quad 0.3 \text{ m}$$
NaHSO$_3$ (r^2 = 0.99), and
$$\ln(A_{1020}/A_{1050}) = 885(\pm59)/T - 1.96(\pm0.19) \quad \text{at} \quad 0.4 \text{ m}$$
NaHSO$_3$ (r^2 = 0.98).

We note that if the bisulfite dimer (S$_2$O$_5^{2-}$) were to contribute significantly to the ~1050 cm^{-1} band, a systematic decrease in values of A_{1020}/A_{1050} with increasing [NaHSO$_3$] at any given temperature would be expected. Such a relationship could not be resolved within the estimated error of our data. For example, at 25 °C we obtain A_{1020}/A_{1050} = 2.46 ± 0.25 at 0.2 m, 2.56 ± 0.18 at 0.3 m, and 2.78 ± 0.24 at 0.4 m NaHSO$_3$ (Table 2).

Fig. 4b-c also include our determinations of A_{1020}/A_{1050} with temperature from experiments performed under different solution compositions and/or within different spectroscopic cells. Fig. 4b includes data from our experiment with NaCl added to increase ionic strength (0.2 m NaHSO$_3$, 0.8 m NaCl, calculated ionic strength of μ = 1.0 m). Our determinations of A_{1020}/A_{1050} with and without added NaCl at 0.2 m NaHSO$_3$ are not resolvable from one another within the estimated errors and yield essentially identical trends with temperature. Fig. 4c additionally includes data from the time series experiments and our sapphire window experiments (all performed at 0.3 m NaHSO$_3$). When taken together these yield comparable values for A_{1020}/A_{1050} at their respective temperature values. Experiments performed in the sapphire window cell at different pH values do not show any systematic trends or differences with pH, and yield: A_{1020}/A_{1050} = 2.78 ± 0.15 at pH = 4.4 (unadjusted), A_{1020}/A_{1050} = 2.69 ± 0.06 at pH = 3.8, and A_{1020}/A_{1050} = 3.17 ± 0.12 at pH = 3.3. The latter value of A_{1020}/A_{1050} corresponding to solution of pH = 3.3 is relatively high but on the upper end of the range obtained at 25 °C in the time series experiments performed in FSC and at a similar NaHSO$_3$ concentration (0.3 m).

4. DISCUSSION

4.1. Estimate of the bisulfite isomerization quotient (Q$_i$)

Given our assignments of the ~1020 and ~1050 cm^{-1} symmetric S-O stretching (v_s) bands to the (HO)SO$_2^-$ and (HS)O$_3^-$ isomers, respectively, and our assumption that these bands have similar Raman cross sections for analogous vibrations, we estimate the bisulfite isomer quotient (Q_i) as A_{1020}/A_{1050} (Eq. (6)). There is no evidence that A_{1020}/A_{1050} varies as a function of time. These data indicate, therefore, that the solutions were at equilibrium at the time of measurement. Moreover, there is no clear evidence that A_{1020}/A_{1050} varies significantly as a function of sodium bisulfite concentration at any given temperature over [NaHSO$_3$] = 0.2–0.4 m. Thus, all data collected under temperature-controlled conditions (i.e., in fused silica
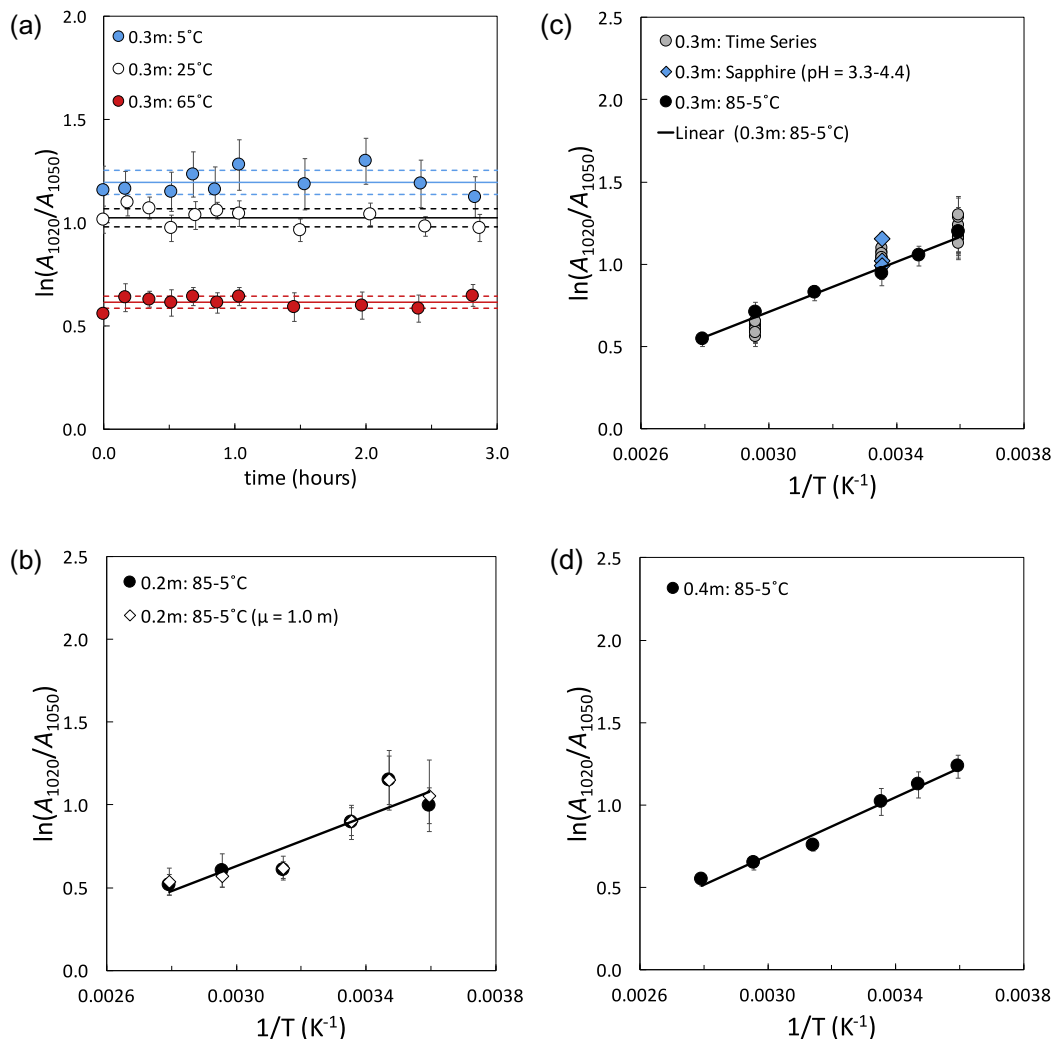
Fig. 4. (a-d): Determinations of A_{1020}/A_{1050} expressed as the natural logarithm from each of our experimental sets: (a) A_{1020}/A_{1050} as a function of time from our time series study; (b) A_{1020}/A_{1050} as a function of temperature from 0.2 m NaHSO₃ solutions with (white diamonds) and without (black circles) added ionic strength (NaCl); (c) A_{1020}/A_{1050} as a function of temperature from 0.3 m NaHSO₃ solutions, where results from our room temperature sapphire window cell experiments (blue diamonds; assumed 25 °C for plotting) and time series experiment (grey circles) are also shown; (d) A_{1020}/A_{1050} as a function of temperature from 0.4 m NaHSO₃ solutions. The error bars on each data point indicate the standard deviation of the mean estimated from our peak fitting exercise.

capsules) in pure NaHSO₃ solutions were incorporated to obtain the following temperature dependence of the quotient via least squares linear regression (Fig. 5; 50 determinations of A_{1020}/A_{1050} in total):

$$\ln (Q_i) = \frac{878.59(\pm 32.98)}{T} - 1.9642(\pm 0.1081) \qquad (7)$$

T indicates temperature in Kelvin and Q_i is dimensionless (note: extra significant figures are given for the linear coefficients to minimize rounding errors). This relationship is expected to be valid over the conditions (0.2–0.4 m NaHSO₃) and temperature range studied (278–358 K, or 5–85 °C). From Eq. (7), Q_i varies from 3.30 ± 0.53 at 5 °C to 1.63 ± 0.23 at 85 °C, and we obtain a value of $Q_i = 2.67 \pm 0.41$ at 25 °C (i.e., relative error on Q_i of 14–16%; errors in Q_i are estimated from the propagation of the stan-

dard errors on the slope and y-intercept in Eq. (7), which yield larger error estimates in Q_i than those estimated from 95% confidence intervals). This translates to a mole fraction ratio of (HO)SO₂⁻ to (HS)O₃⁻ that ranges from 0.77:0.23 to 0.62:0.38 over 5 to 85 °C, respectively (±0.03 for each mole fraction). Eq. (7) does not include data from the experiment performed with added ionic strength (0.2 m NaHSO₃, 0.8 m NaCl; μ = 1.0 m) due to it having a different solution composition. Experiments performed in the sapphire window cell are omitted from this regression due to lack of precise temperature control for these measurements.

The thermodynamic quantities of ΔH°_{rxn}, ΔG°_{rxn} and ΔS°_{rxn} for the isomerization reaction may be estimated from our quotient determination. If we assume that the quotient is equivalent to the equilibrium constant K and correspondingly that activity coefficients are unity (or at

least their ratio is unity for the isomers), the slope of Eq. (7) would imply an enthalpy of the isomerization reaction at standard state of $\Delta H°_{rxn} = -1.75 \pm 0.07$ kcal/mol (-7.3 ± 0.3 kJ/mol). The estimated values for $\Delta H°_{rxn}$ may range from -1.4 to -2.1 kcal/mol (-5.7 to -8.9 kJ/mol) based on the computed 95% confidence intervals. Similarly, Eq. (7) would imply a free energy of the isomerization reaction at standard state of $\Delta G°_{rxn} = -0.58 \pm 0.09$ kcal/mol (or -2.2 ± 0.4 kJ/mol), and an entropy of the isomerization reaction of $\Delta S°_{rxn} = -3.9 \pm 0.2$ cal mol^{-1} K^{-1} (or -16.3 ± 0.9 J mol^{-1} K^{-1}).

4.2. Comparison to other estimates of Q_i

The values of Q_i compare well to the relatively recent value reported by Risberg et al. (2007) of $Q_i = 2.7 \pm 0.5$ at 25 °C that is based on the fitting of a sulfur K-edge XANES spectrum collected from a solution of 0.05 M NaHSO$_3$ at pH = 3.9 (Fig. 5). Their fitting procedure required constraints on the individual XANES spectra for each of the two bisulfite isomers, which they obtained from density functional theory calculations. Risberg et al. (2007) were able to quantify a quotient only at 25 °C, but found that features attributable to the (HS)O$_3^-$ isomer increased relative to those of the (HO)SO$_2^-$ isomer with increasing temperature over 4–70 °C that is in qualitative agreement with our own and other's observations using other forms of spectroscopy (Horner and Connick, 1986; Littlejohn et al., 1992).

The values for Q_i reported by Littlejohn et al. (1992) based on a similar interpretation of Raman spectra as in the present study yield different apparent values for Q_i and a different temperature dependence (Fig. 5) with ln $(Q_i) = 1581(\pm 197)/T - 3.64(\pm 0.66)$ ($\sim$274–340 K; 11 data points digitally extracted from their figure). These data suggest $Q_i \sim 5.3$ at 25 °C. Very large errors in Q_i are obtained when the standard errors from the slope and y-intercept are propagated through to the computation of a quotient at any given temperature (± 4.9 at 25 °C), but errors estimated from our own computed 95% confidence intervals from their data are smaller (± 0.7 at 25 °C). Littlejohn et al. (1992) do not make clear which reported solution conditions correspond to those used to obtain spectra for the estimation of the isomer quotient, but we might assume that they are on the lower end of their reported NaHSO$_3$ concentrations (0.15 and/or 0.5 m NaHSO$_3$). The temperature dependence of the quotient observed by Littlejohn et al. (1992) is slightly more pronounced than observed here and suggests $\Delta H°_{rxn} = -3.1 \pm 0.4$ kcal/mol for the isomerization reaction with a range spanning -1.9 to -4.4 kcal/mol from 95% confidence intervals.

Littlejohn et al. (1992) report to have estimated Q_i from their extraction of the equivalent of A_{1020}/A_{1050} from their Raman spectra (cf. Eq. (6)), but unfortunately do not provide any details on their peak fitting procedure. In order to make a rough assessment of their Raman data to explore why the two studies obtain such different values for the isomer quotient using a similar approach, two spectra from one of their figures that are reported to have been collected from a solution containing 0.15 m NaHSO$_3$ at 2 °C and 67 °
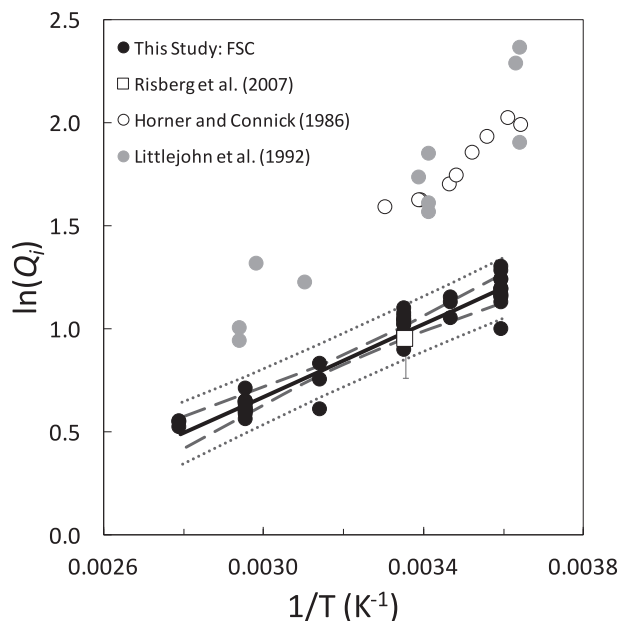

Fig. 5. Our estimation of the bisulfite isomer quotient ($Q_i = $[(HO)SO$_2$]/[(HS)O$_3^-$]) as a function of temperature from experiments prepared in FSCs with pure NaHSO$_3$ solutions (0.2–0.4 m) alongside previous experimental estimates that utilized various spectroscopic techniques (XANES = Risberg et al., 2007; Raman = Littlejohn et al., 1992; 17O NMR = Horner and Connick, 1986). The solid black line indicates the least squares linear regression of our data (i.e., Eq. (7) in the text) and the dashed curves indicate the computed 95% confidence intervals (heavy dashed curves) and 95% prediction intervals (dotted curves).

C were digitally extracted and subjected to a peak fitting exercise to estimate the integrated intensities of the $\sim$1020 and 1050 cm^{-1} bands in a manner similar to that applied to the spectra in the present study (Fig. 6). This exercise yields values for A_{1020}/A_{1050} on the order of 3.1 ± 0.5 at 2 °C and $A_{1020}/A_{1050} \sim 1.5$ at 67 °C (Fig. 6), which is in much closer agreement to the values obtained in the present study. We note that the 2 °C spectra seemed to require the inclusion of an additional feature on the high frequency side of the $\sim$1050 cm^{-1} band analogous to the present spectra collected over 5–85 °C to improve fit quality; otherwise, the estimated values of A_{1020}/A_{1050} from their spectra at this temperature are even lower. It is thus difficult for us to reconcile the reported values of Q_i from Littlejohn et al. (1992) with the information provided in their paper.

Horner and Connick (1986) obtained isomer quotients based on the interpretation of ^{17}O NMR spectra collected from NaHSO$_3$ solutions ([HSO$_3^-$] = 0.20 and 0.45–0.46 m) prepared at different pH (pH* = 3.0 and 4.98; *measured at room temperature). They additionally adjusted their NaHSO$_3$ solutions with NaCl to have total ionic strength of $\mu = 1.0$ m, and used ^{17}O-enriched water for their measurements. The regression of their reported Q_i as a function of temperature yields ln$(Q_i) = 1441(\pm 150.4)/T - 3.241$ (± 0.5249) (274–302 K; 9 data points), which yields a value of $Q_i \sim 4.9$ at 25 °C. The errors in Q_i obtained from the propagation of errors associated with the slope and y-
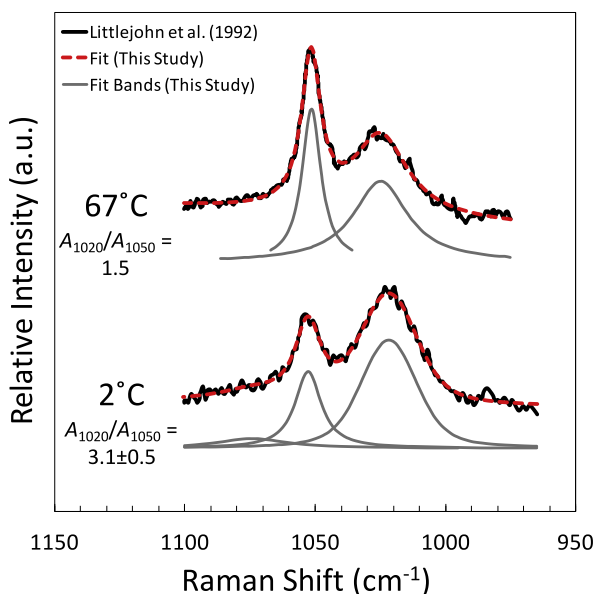
Fig. 6. Raman spectra digitally extracted from Littlejohn et al. (1992) (black curves) that we subjected to multipeak curve fitting (red dashed curve) for quantification of component model Raman bands (offset grey curves) in an analogous manner as the Raman spectra reported in the present study. The reported solution conditions are 0.15 m NaHSO$_3$ (Littlejohn et al., 1992). The estimates for the isomer quotient ($Q_i \sim A_{1020}/A_{1050}$) derived from our fits yield $A_{1020}/A_{1050} = 3.1 \pm 0.5$ at 2 °C and 1.5 at 67 °C, and are very comparable to the results of the present study. We note that the 2 °C spectra appear to require an additional band on the high frequency shoulder of the ~1050 cm^{-1} band similar to the present study (cf. Fig. 3); without this band the estimates for Q_i are even lower in magnitude and, thus, further from agreeing with values of Q_i originally reported by Littlejohn et al. (1992). (For interpretation of the references to colour in this figure legend, the reader is referred to the web version of this article.)

intercept of the least squares linear regression are quite large (± 3.6 at 25 °C), but are smaller when estimated from our own computations of 95% confidence intervals (± 0.3 at 25 °C). The apparent enthalpy of the isomerization reaction from their data is $\Delta H°_{rxn} = -2.9 \pm 0.3$ kcal/mol with a range of -2.08 to -3.65 kcal/mol from computed 95% confidence intervals.

The approach of Horner and Connick (1986) relied on a more elaborate interpretation of experimental spectra compared to either the Raman or XANES approaches described previously (this study; Littlejohn et al., 1992; Risberg et al., 2007), which appears to be due to complications introduced into the spectra related to oxygen isotope exchange among S(IV) solutes and water. In short, they found that the peaks attributable to S(IV) compounds in ^{17}O NMR spectra varied substantially as a function of pH (3–5), which they interpreted to broadly reflect varying oxygen isotope exchange rates among bisulfite/S(IV) species and water over this pH range. They observed two overlapping peaks centered at ~175 and ~195 ppm at intermediary pH values (i.e., pH = 4.44) that they assigned to (HS)O$_3^-$ and (HO)SO$_2^-$, respectively, based on their apparent relative oxygen isotope exchange rates with water

as inferred from the relative changes in peak dimensions with pH and assuming the HO-isomer exchanges more readily than the HS-isomer. At the end member pH values of 3 and 5, only singular S(IV) peaks were observed: ~173 ppm at pH = 3 (attributed solely to (HS)O$_3^-$ by the authors), and ~195 ppm at pH 5, where the latter was interpreted to be a coalesced band comprised of all S(IV) species present under these conditions (i.e., (HO)SO$_2^-$, (HS)O$_3^-$, S$_2$O$_5^{2-}$, and SO$_3^{2-}$). Ultimately, they estimated the isomer quotient from the ratio of the peak areas of the coalesced peak at pH = 5 (193 ppm) to that of the ~173 ppm peak observed at pH = 3 following $Q_i = [HSO_3^-]_{TOTAL}/[(HS)O_3^-] - 1$ (where $[HSO_3^-]_{TOTAL} = [(HS)O_3^-] + [(HO)SO_2^-]$), with corrections made to the coalesced band for the pH difference and the contribution of other S(IV) species based on calculated mole fractions from the available dissociation and bisulfite dimerization quotients at $\mu = 1.0$ m.

It is ultimately unclear why we obtain such different values for the isomer quotient than Horner and Connick (1986). One possibility that we considered relates to differences in solution composition in our experiments including ionic strength and pH. Our one experiment performed with added ionic strength (0.2 m NaHSO$_3$, 0.8 m NaCl; $\mu = 1.0$ m) was an attempt to replicate the solution conditions of Horner and Connick (1986) with the caveat of the much different bulk isotopic composition of water that was used for the ^{17}O NMR measurements. Our experiment with added NaCl did not yield significantly different values for A_{1020}/A_{1050} as a function of temperature from those obtained in the experiment performed without added NaCl (Fig. 4b). It thus appears that the effect of ionic strength on the estimation of Q_i is not resolvable with our dataset. Our room temperature experiments in the sapphire window cell at different pH values were an attempt to evaluate whether pH has a pronounced effect, since their estimation of the quotient is ultimately derived from spectra and calculations at lower pH (pH = 3). There does not appear to be a significant difference with pH based on our Raman determinations over a few different values over pH = 3.3–4.4. A slightly higher value for A_{1020}/A_{1050} was found for the pH = 3.3 solution (yielding $Q_i = 3.17 \pm 0.12$), but still nowhere near the values reported by Horner and Connick (1986) that are ca. $Q_i \sim 5$ at 25 °C.

Horner and Connick (1986) noted that peak fitting exercises applied to spectra that contained the two overlapping peaks centered at ~195 ppm and ~175 ppm (attributed to each of the isomers) yielded peak area ratios (195 ppm:175 ppm) on the order of 5–10, but preferred to not use these values for estimating Q_i. Their preference appears to be due to the dramatic changes observed in the relative dimensions of these peaks as a function of pH in the ^{17}O NMR spectra that may have hindered a precise or accurate determination. For the sake of the exercise, we digitally extracted from one of their figures the spectra collected at pH = 4.44 from solutions of 0.2 m NaHSO$_3$ ($\mu = 1.0$ m; temperature range specified as 4–10 °C), and performed a simple peak fitting exercise. Given the pH and conditions specified, we would expect this spectrum to potentially be the most representative of a relatively pure HSO$_3^-$ solution (i.e., minimal presence of other S(IV) species) with the caveat of the extra components added for

increased ionic strength. This is also the pH that is the most similar to most of our own experimental data, and is consistent with the pH of an unadjusted sodium bisulfite solution prepared from $Na_2S_2O_5$ salts. We obtain peaks centered at 176 ppm and 195 ppm (consistent with their reported chemical shifts) and peak area ratio of the 195 ppm peak to the 176 ppm peak of $\sim$3.8, which is lower than the range they reported to have obtained from their own curve fitting procedures (5–10), and when directly taken as an estimate for Q_i is much lower than their other estimates. This estimate of Q_i approaches the upper bounds of our Raman constraints over their specified temperature range for the spectrum of 4–10 °C.

It is possible that our assumption of similar Raman cross sections for the analogous symmetric S-O stretching vibrational frequencies for the two isomers is in error. This assumption may not be exactly correct but it is probably reasonable. For example, this assumption can be further applied to estimate the mole% of $SO_{2(aq)}$ in equilibrium with bisulfite (($HO)SO_2^- + (HS)O_3^-$) in the solutions from the two pH adjusted experiments (pH = 3.3 and 3.8) in the sapphire window cell performed at room temperature via the following:

mole fraction of $SO_{2(aq)}$ (%)

$$= \frac{A_{1150}}{A_{1020} + A_{1050} + A_{1150}} \times 100. \quad (8)$$

Here, the integrated intensities (A) correspond to the symmetric stretch (S-O) vibrational frequencies for the species, and the denominator is the sum of A for all expected species in solution (($HO)SO_2^- + (HS)O_3^- + SO_{2(aq)}$). We obtain $\sim$1.4% $SO_{2(aq)}$ at pH = 3.8 and 3.6 ($\pm$0.2)% $SO_{2(aq)}$ at pH = 3.3 (Table 4), which is in good agreement with the expected values of 1.1% and 3.5%, respectively, from the thermodynamic constant of the SO_2 hydrolysis reaction to form bisulfite at standard state (i.e., Eq. (2), $K = 10^{-1.86}$; e.g., Goldberg and Parker, 1985; Millero et al., 1989). This exercise suggests that the different bonding environments between $SO_{2(aq)}$ and the bisulfite isomers may not lead to substantially different Raman cross sections for the analogous vibrational modes. It is also noted that these values for the intensities take into consideration the uncertain position and dimensions of the interfering band via our peak fitting protocol, and our simple exercise using Eq. (8) may additionally be taken to suggest that our treatment of this band in our peak fitting procedure is adequate within the associated errors for estimating equilibrium constants for the associated species.

It is also possible that the number of bands used for curve fitting in the ca. 1000–1200 cm^{-1} region is incomplete, and this may have biased the relative peak area determinations of the $\sim$1020 and 1050 cm^{-1} bands. However, we do not find evidence or justification for the inclusion of any other bands into our peak fitting procedure at this time. It seems unlikely that the superposition of a band from the bisulfite dimer ($S_2O_5^{2-}$) at $\sim$1050 cm^{-1} could explain the apparent discrepancy between our results and those of Horner and Connick (1986), given its very low expected concentration under the solution conditions (<1–2% of total S(IV); e.g., Connick et al., 1982; Beyad et al., 2014) and the lack of observation of other bands attributable to

the dimer in the Raman spectra. All else being equal, the dimer would have to contribute to 45–50% of the total area of the $\sim$1050 cm^{-1} band in order for our quotient estimation to match the isomer quotient of Horner and Connick (1986) at 25 °C, which does not seem reasonable.

4.3. Implications for Sulfur Isotope Fractionations in Aqueous Solutions

Eldridge et al. (2016) recently provided estimates for compound specific sulfur isotope fractionation factors (i.e., β-factors) for a number of sulfur compounds modeled in 30–34 H_2O clusters for predicting equilibrium isotope fractionation factors among aqueous sulfur compounds. This includes β-factors for compounds in the S(IV) system. The results of these calculations were coupled with the available constraints on the bisulfite isomer quotient (Horner and Connick, 1986; Littlejohn et al., 1992; Risberg et al., 2007) to estimate bulk fractionation factors between bisulfite and other S(IV) species. This exercise included a comparison to the available experimental constraints (Eriksen, 1972) where an isotope fractionation factor was measured between total aqueous bisulfite and SO_2 in the gas phase via a distillation method. Eriksen (1972) obtained a fractionation factor of $1000 \times \ln(^{34}\alpha_{bulk\ bisulfite/SO2(g)}) = 10.9 \pm 1.4‰$ at 25 °C, and was unable to resolve a significant temperature dependence over 25–45 °C (note: $^{34}\alpha_{bulk\ bisulfite/SO2(g)} = (^{34}S/^{32}S)_{bulk\ bisulfite}/(^{34}S/^{32}S)_{SO2(g)}$). We can perform a similar comparison using the new Raman constraints on the isomer quotient provided in the present study.

In Fig. 7a, the experimental data of Eriksen (1972) are shown along with the theoretical fractionation factors calculated from Eldridge et al. (2016). The curve representing a total (or "bulk") fractionation factor between total bisulfite ($HSO_3^- = (HO)SO_2^- + (HS)O_3^-$) and gaseous SO_2 is calculated via the following equation:

$$^{34}\alpha_{bisulfite(bulk)/SO_{2(g)}} = \frac{\frac{Q_i}{(1+Q_i)}{}^{34}\beta_{(HO)bisulfite} + \frac{1}{(1+Q_i)}{}^{34}\beta_{(HS)bisulfite}}{{}^{34}\beta_{SO_{2(g)}}}, \quad (9)$$

where the ^{34}β-factors as a function of temperature are from the theoretical calculations of Eldridge et al. (2016), and Q_i is calculated as a function of temperature from Eq. (7). The bounding dashed curves represent the estimated uncertainty based solely on the propagated errors of the slope and y-intercept in Eq. (7) into the calculation of the fractionation factor. Our calculated curve passes directly through the experimental data of Eriksen (1972) and yields essentially identical values within the estimated errors. We emphasize that the curve based on Eq. (9) and the data points from Eriksen (1972) in Fig. 7a represent two completely independent approaches to obtaining $^{34}\alpha_{bulk\ bisulfite/SO_{2(g)}}$, and each appears to yield similar values. We note that if the quotient from Horner and Connick (1986) is used instead in our implementation of Eq. (9), the predicted bulk fractionation factors are generally lower in magnitude ($1000 \times \ln(^{34}\alpha_{bulk-bisulfite/SO2(g)}) = 8.8 \pm 2.4‰$ at 25 °C) but are within the estimated error (cf. Eldridge et al., 2016).
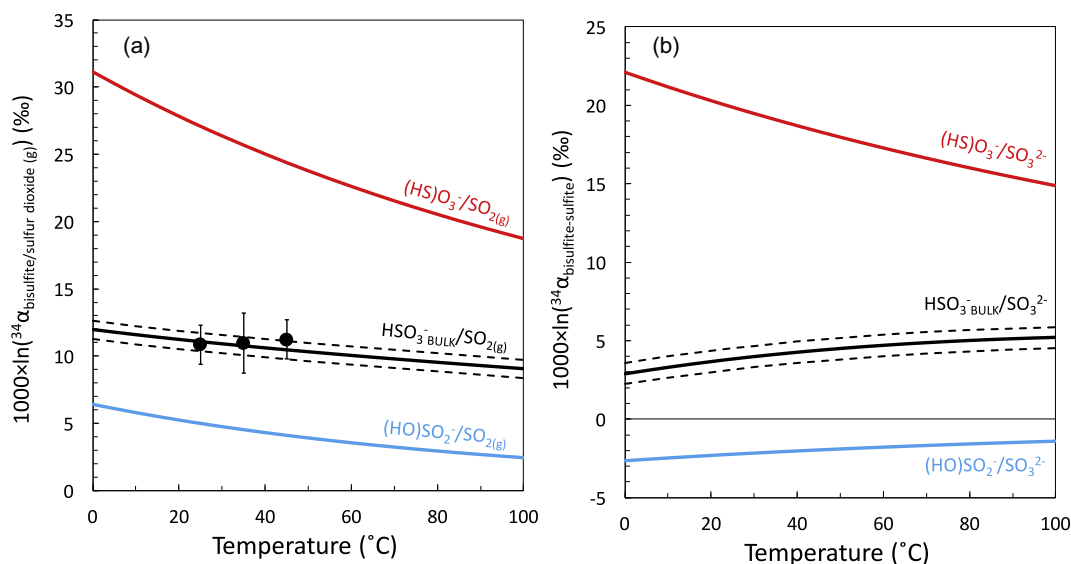
Fig. 7. (a-b): Equilibrium sulfur isotope fractionation factors among compounds in the S(IV) system that incorporates our new estimates for Q_i. (a) Fractionation factor between aqueous bisulfite compounds and gaseous sulfur dioxide: The black circles are the experimental data of Eriksen (1972), the blue and red curves indicate isomer-specific fractionation factors from the theoretical calculations of Eldridge et al. (2016), and the black curve is a bulk fractionation factor that is based on our new values for Q_i and the theoretical fractionation factors (following Eq. (9) in the text), which is found to be indistinguishable from Eriksen (1972). (b) Predictions of fractionation factors between the bisulfite isomers and sulfite *sensu stricto* (SO_3^{2-}) following an analogous color scheme to panel (a), where the red and blue curves are the isomer-specific fractionation factors from Eldridge et al. (2016), and the black curve is the fractionation factor between bulk bisulfite and sulfite *sensu stricto* that incorporates our new estimate for Q_i (following Eq. 10 in the text). (For interpretation of the references to colour in this figure legend, the reader is referred to the web version of this article.)

Updated predictions for the analogously calculated fractionation factors between bisulfite compounds and sulfite *sensu stricto* (SO_3^{2-}) are shown in Fig. 7b. These calculations are relevant to circumneutral pH solutions where all three species are expected to be present in significant abundance. The curve representing a "bulk" fractionation factor between total bisulfite ($HSO_3^- = (HO)SO_2^- + (HS)O_3^-$) and sulfite ($SO_3^{2-}$) is calculated via the following equation:

$$^{34}\alpha_{bisulfite(bulk)/SO_3^{2-}} = \frac{\frac{Q_i}{(1+Q_i)} {}^{34}\beta_{(HO)bisulfite} + \frac{1}{(1+Q_i)} {}^{34}\beta_{(HS)bisulfite}}{^{34}\beta_{SO_3^{2-}}}.$$

(10)

As before, the $^{34}\beta$-factors as a function of temperature are from the theoretical calculations of Eldridge et al. (2016), and Q_i is calculated as a function of temperature from our Eq. (7). The same basic conclusions drawn by Eldridge et al. (2016) regarding the profound effect of bisulfite isomerization on isotope fractionations stand, where the minor ($HS)O_3^-$ isomer plays a dominant role in influencing bulk fractionation behavior between bisulfite and other compounds including the fractionation magnitudes (Fig. 7a and b), the apparent temperature dependence (Fig. 7a and b), and even apparent direction in the case of the bisulfite/sulfite fractionations (Fig. 7b). Note that the bulk fractionation factor between total bisulfite and sulfite *sensu stricto* is predicted to have an apparent inverse temperature dependence (fractionation magnitude increases with increasing temperature) over ca. 5–85 °C that is contrary to the temperature dependence of either individual isomer's fractionation factors. This is due simply to the relative magnitudes and directions of the fractionation factors involved for each isomer, and the fact that the minor isomer increases in proportion to total bisulfite with increasing temperature. We note that the application of Q_i from the determinations of Horner and Connick (1986) to Eq. (10) generally yields lower magnitude bulk fractionation factors ($1000 \times \ln(^{34}\alpha_{bulkbisulfite/SO2(g)}) = 1.5 \pm 2.5‰$ at 25 °C) but are still generally within the estimated error of the predictions made with our values of Q_i.

Eldridge et al. (2016) hypothesized that ionic strength may be an important factor in influencing sulfur isotope fractionations in bisulfite systems due to the apparent differences in the isomer quotient obtained by ^{17}O-NMR from bisulfite solutions prepared at $\mu = 1.0$ m (Horner and Connick, 1986) and XANES spectroscopy from bisulfite solutions that were prepared close to $\mu \sim 0$ m (Risberg et al., 2007). As far as we are aware, the present study is the only study to apply the same method and approach to estimating the isomer quotient from aqueous bisulfite solutions prepared at different ionic strength (Fig. 4b). We are unable to resolve any differences in our estimation of Q_i as a function of ionic strength over the range we have investigated. This might tentatively suggest that the spectroscopic approach and the underlying assumptions made to quantify the quotient via the interpretation of experimental spectra may have played a larger role in the apparent differences obtained in Q_i than differences in ionic strength in the investigated aqueous bisulfite solutions. This does not necessarily rule out a role for ionic strength in influencing speciation (e.g., *via* ion pair formation) and therefore isotope fractionations in bisulfite systems, but

simply means that the effect that ionic strength may have on Q_i over the range we have studied is within the estimated errors of the present Raman-based approach.

4.4. Bisulfite compounds and dissimilatory sulfate reduction

Dissimilatory sulfate reduction is a dominant anaerobic respiration process in Earth surface environments (e.g., Bowles et al., 2014) that has strongly influenced the chemical and isotopic make-up of the sedimentary rock record (Canfield, 2001, 2004; Farquhar et al., 2010; Rickard, 2014), and whose antiquity in Earth history may be comparable to the sedimentary rock record itself (*cf.* Shen et al., 2001, 2009; Shen and Buick, 2004; Ueno et al., 2008; Wacey et al., 2011; Johnston, 2011). The sulfur isotope fractionations associated with sulfate reduction and their major controls are therefore critical to interpreting the geologic rock record, and ultimately arise from factors that influence the net expression of isotope fractionations associated with the step-wise intracellular transformation of sulfur through the metabolism. Within the cellular membrane of sulfate reducing microorganisms, sulfate reduction can be described in terms of four overall steps that are mediated by different enzymes and/or enzyme sub-units that involve a handful of sulfur intermediates (*cf.* Parey et al., 2013; Santos et al., 2015): (1) sulfate activation to adenosine phosphosulfate (APS) via the enzyme ATP-sulfurylase, (2) APS reduction via the enzyme adenosine-5′-phosphosulfate reductase producing the aqueous sulfite compounds, (3) the binding of aqueous sulfite to the active siroheme site of the enzyme dissimilatory sulfite reductase (Dsr; comprised of subunits DsrAB that contains the sirohemes, and DsrC) followed by its step-wise reduction (and dehydration) to produce a siroheme-bound zero-valent sulfur atom, and (4) the detachment reaction of the zero-valent sulfur atom from DsrAB involving two conserved cysteines of a DsrC subunit where it is then elsewhere reduced to produce the end product aqueous sulfide (as H_2S/HS^-) (Santos et al., 2015). Sulfite compounds are key in the sulfate reduction metabolism because they are among the species that directly interact with the active sites of enzymes (especially Dsr) in the reactions that comprise the central sulfur redox core of the metabolism.

From the available experiments performed with sulfate reducers in continuous pure culture, the sulfur isotope fractionation magnitudes (in terms of $^{34}\varepsilon_{sulfate-sulfide} = (^{34}\alpha_{sulfate-sulfide} - 1) \times 1000$) between extracellular sulfate and sulfide appear to approach upper and lower bounds that span a range of roughly 40–50‰ at ambient temperature ($\sim$20 °C) that depend critically on the cell specific sulfate reduction rate (csSRR; Sim et al., 2011a, 2011b; Leavitt et al., 2013). The wide range of fractionation that is possible for the metabolism under different growth conditions is informative and may lend interpretive power to natural variability in modern systems and the rock record. It has long been recognized that the isotope fractionations associated with each of the individual steps within the metabolism represent important constraints to include in models that attempt to connect the experimentally observed net fractionations associated with the metabolism to the underpinning intra-

cellular enzyme-mediated steps (e.g., Rees, 1973; Brunner and Bernasconi, 2005; Johnston et al., 2007; Bradley et al., 2011; Wing and Halevy, 2014), but the isotope effects associated with enzyme-mediated transformations are among the least well-constrained and are often incompletely treated in current models. Recently, Leavitt et al. (2015) reported the first experimental constraints on the sulfur isotope fractionations associated with sulfite reduction via dissimilatory sulfite reductase, which were performed *in vitro* utilizing Dsr with the DsrC subunit inactive (representing solely DsrAB) isolated from the sulfate reducer *Desulfovibrio vulgaris* (strain Hildenborough). The solution conditions for these *in vitro* experiments were carefully chosen to be similar to *in vivo* (i.e., intracellular) conditions of the organism in proximity to its optimal growth temperature (*D. vulgaris*: pH = 7.1, T = 20 or 31 °C; Leavitt et al., 2015). Leavitt et al. (2015) were able to constrain a fractionation factor associated with sulfite reduction by DsrAB isolated from *D. vulgaris* of about $^{34}\varepsilon_{sulfite-sulfur} = 15 \pm 2$‰ from these experiments. This fractionation factor derived from the novel approach of Leavitt et al. (2015) is an important step towards evaluating how enzyme-level processes may translate into isotopic fractionations among geologically relevant sulfur phases in natural environments.

The key point to make in the context of the present study is that the sulfite pool that is drawn upon for binding to the siroheme active sites of DsrAB for their overall reduction to a zero-valent sulfur atom (i.e., Step 3 above) within the cellular membrane of sulfate reducers has a much more complex molecular and isotopic composition than is generally considered. For example, under the reported conditions of the Leavitt et al. (2015) experiments with DsrAB isolated from *D. vulgaris* (pH = 7.1, T = 20 or 31 °C), we predict that the sulfite solution used was comprised of three sulfite compounds in major relative abundance: $\sim$47–45% SO_3^{2-}, $\sim$39% $(HO)SO_2^-$, and $\sim$14–16% $(HS)O_3^-$ over 20–31 °C (calculated utilizing data from the present study and Goldberg and Parker, 1985; Millero et al., 1989). In principle, the three different sulfite compounds present under these conditions will have distinct mechanisms of binding to the siroheme active site of DsrAB due to their structural differences (i.e., different reaction coordinates associated with $Fe-SO_3$ bond formation) that can be accompanied by their own distinct primary kinetic isotope effects. Therefore, the net fractionation associated with *bulk* sulfite compound reduction by dissimilatory sulfite reductase is likely to contain contributions from more than one primary kinetic isotope effect that is at least related to the binding of the different sulfite compounds. This mechanistic view of the reactions between SO_3^{2-}/$(HO)SO_2^-$/$(HS)O_3^-$ and the active sites of DsrAB and other enzymes will likely be necessary in order to fully evaluate the isotope effects associated with these key steps of the sulfate reduction metabolism.

We have previously hypothesized that the $(HS)O_3^-$ isomer may have a particularly distinct reaction mechanism with respect to its binding to the active site of Dsr because this species lacks the lone pair of electrons on the sulfur atom that characterizes sulfite *sensu stricto* (SO_3^{2-}) that facilitate the formation of a bond between the sulfur atom

in sulfite to the iron atom of the siroheme active site (Eldridge et al., 2016). We have additionally speculated that this may be the basis for the discrimination of the $(HS)O_3^-$ species at the level of the active site due to a resulting kinetic inhibition towards binding (Eldridge et al., 2016). If indeed not all sulfite compounds are chemically equal with respect to the active sites of Dsr, the complex speciation of sulfite could additionally influence the apparent sulfur isotope fractionations associated with the overall reduction of sulfite compounds by Dsr. For example, if the reaction of the $(HS)O_3^-$ species is indeed kinetically inhibited due to its structure, then the enzyme would be sampling only a portion of the total sulfite pool that may have a sulfur isotopic composition that is distinct from the bulk sulfite isotopic composition. The magnitude of such imparted effects would depend on the amount of $(HS)O_3^-$ that is present in intracellular media, because the isotopic composition of the $(HS)O_3^-$ isomer is predicted to be significantly distinct from SO_3^{2-} and $(HO)SO_2^-$ when they are in isotopic equilibrium with each other (cf. Fig. 7b). The sulfur isotope exchange rates among the aqueous sulfite compounds are not presently known, and so it is not clear how they compare to the turnover times of sulfite compounds within sulfate reducers under different growth conditions, but the equilibrium vs. non-equilibrium isotope fractionations among the aqueous sulfite species could be additional variables to consider in the evaluation of the apparent isotope fractionations associated with the enzyme mediated intracellular transformations of mixtures of sulfite compounds.

Sulfite speciation is clearly a strong function of temperature and sulfate reducers may successfully operate over a wide range of temperature. For additional illustration, we calculate the expected speciation of sulfite compounds at neutral pH as a function of temperature (Fig. 8) in order to obtain a rough sketch of the molecular composition of S(IV) that might be expected under simplified intracellular conditions under different temperatures. The calculations in Fig. 8 were carried out by determining the neutral pH of water using the H_2O dissociation equilibrium constant as a function of temperature (varies from pH = 7.4–6.1 over 0–100 °C; e.g., Bandura and Lvov, 2006), and then calculating the mole fraction of S(IV) compounds expected at these pH/temperature conditions using the thermodynamic data for Equations (2) and (3) (Goldberg and Parker, 1985; Millero et al., 1989) and Q_i from Eq. (7). We use the optimal growth temperatures of two model sulfate reducing organisms (*Desulfovibrio vulgaris* and *Archaeoglobus fulgidus*, ca. 37 and 83 °C, respectively; Klenk et al., 1997; Huang et al., 2004) as points of comparison. Under neutral pH conditions over ca. 0–100 °C, the two bisulfite isomers and sulfite *sensu stricto* are expected to be present in major abundance, and bisulfite compounds are in the majority >15–20 °C (Fig. 8). It is perhaps most striking to note that at the optimal growth temperature of the thermophilic *A. fulgidus* (~83 °C) bisulfite is expected to dominate speciation at neutral pH (~95% HSO_3^- vs. ~5% SO_3^{2-}), and the minor bisulfite isomer $(HS)O_3^-$ may comprise ~36% of total S(IV). The predicted equilibrium fractionation factor between the two bisulfite isomers at 83 °C is expected to
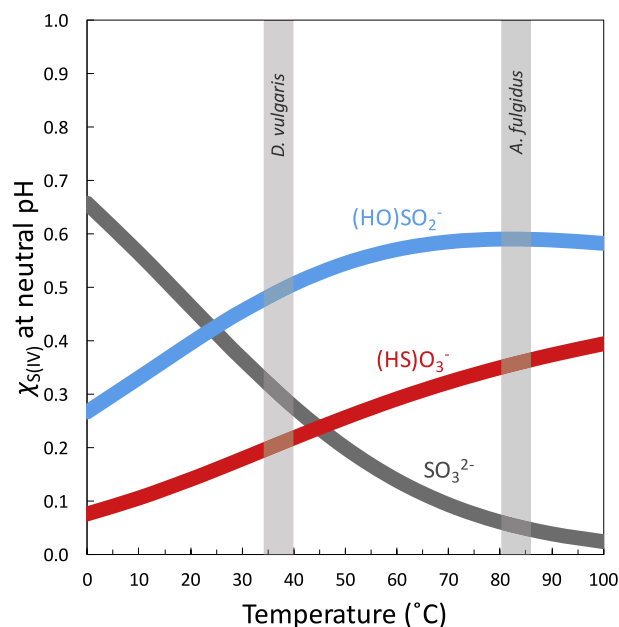

Fig. 8. Calculation of the mole fraction of S(IV) compounds ($\chi_{S(IV)}$) expected under neutral pH conditions as a function of temperature combining previous thermodynamic data (Goldberg and Parker, 1985; Millero et al., 1989; Bandura and Lvov, 2006) and our new values of Q_i. If we assume neutral pH is representative of a simplified intracellular environment within sulfate reducing organisms, we may estimate how temperature influences intracellular S(IV) speciation under the optimal growth temperatures of two model sulfate reducing organisms: *Desulfovibrio vulgaris* (~37 °C) and *Archaeoglobus fulgidus* (~83 °C) (indicated as vertical gray lines). Although not well-known, recent determinations of the intracellular concentration of total S(IV) from *Desulfovibrio alaskensis* by Sim et al. (2017) suggests that they may be sufficiently low such that the bisulfite dimer may be safely ignored (i.e., [S(IV)] ≤ 2 × 10⁻⁵ *m*). We note that the molecular composition of S(IV) is expected to vary considerably over these conditions, which could have implications for enzyme mediated reactions involving these compounds and their apparent overall isotope fractionations (cf. Fig. 7).

be 1000 $\ln(^{34}\alpha_{(HS)bisulfite/(HO)bisulfite}) \sim 17.4\%$ (Fig. 7b; Eldridge et al., 2016), indicating that the two major S(IV) compounds present under these conditions are expected to have significantly distinct sulfur isotope compositions. The profound changes in sulfite speciation as a function of temperature under conditions comparable to the intracellular environment of sulfate reducers may suggest that the different mechanisms of sulfite compound binding to the active sites of enzymes (i.e., SO_3^{2-} vs. $(HO)SO_2^-$ vs. $(HS)O_3^-$) are likely to differ in their relative importance over different temperature regimes, which may additionally have consequences for the isotope fractionations associated with these transformations. Thus, the speciation of sulfite compounds as a function of intracellular conditions should be carefully evaluated in the context of the underpinning mechanisms of the enzyme-mediated sulfite compound transformations that occur as part of the sulfate reduction metabolism.

5. CONCLUSIONS

We report new estimates of the bisulfite isomer quotient as a function of temperature using *in situ* Raman spectroscopy. Our Raman spectra are very similar to those reported from bisulfite solutions in the literature. However, our quantitative interpretation of Raman bands seems to indicate a lower value for the isomerization quotient than has been inferred from previous Raman data (Littlejohn et al., 1992), and is in agreement with the quotient determined from a recent XANES study (Risberg et al., 2007) and in disagreement with those reported in an earlier ^{17}O NMR study (Horner and Connick, 1986). The underlying reasons for these differences are not fully known, but our re-interpretation of earlier Raman spectra (Littlejohn et al., 1992) and a select ^{17}O NMR spectrum (Horner and Connick, 1986) yields values for Q_i that are consistent with the present study. We have implemented our determination of the isomer quotient in sulfur isotope mass balance calculations of sulfite solutions involving different sulfite compounds utilizing recent theoretical calculations of equilibrium sulfur isotope effects (Eldridge et al., 2016), and find that our independent assessment of sulfur isotope fractionations is in excellent agreement with the available experiments (Eriksen, 1972). We additionally revise our predictions for bulk fractionation factors in the SO_3^{2-}, $(HO)SO_2^-$, $(HS)O_3^-$ system over ~0–100 °C. These overall assessments of bulk sulfur isotope fractionation factors involving bisulfite indicate that the minor bisulfite isomer $(HS)O_3^-$ has a strong influence on sulfur isotope fractionation behavior. The speciation of sulfite compounds as a function of solution conditions should, thus, be carefully evaluated in the context of the mechanisms and isotope fractionations associated with the transformation of sulfite compounds, including the enzyme-mediated reactions that occur as part of the highly influential sulfate reduction metabolism. The present study combined with our previous theoretical calculations (Eldridge et al., 2016) may allow for a more detailed evaluation of the molecular composition and sulfur isotope mass balance of sulfite compounds over a wider range of conditions than previously available, including those similar to the intracellular environment of sulfate reducing microorganisms.

ACKNOWLEDGEMENTS

APPENDIX A. SUPPLEMENTARY MATERIAL

Supplementary data associated with this article can be found, in the online version, at https://doi.org/10.1016/j.gca.2017.10.005.

REFERENCES

Bak F. and Pfennig N. (1987) Chemolithotrophic growth of Desulfovibrio sulfodismutans sp. nov. by disproportionation of inorganic sulfur compounds. *Arch. Microbiol.* **147**, 184–189.

Bandura A. V. and Lvov S. N. (2006) The ionization constant of water over wide ranges of temperature and density. *J. Phys. Chem. Ref. Data* **35**, 15–30.

Beyad Y., Burns R., Puxty G. and Maeder M. (2014) A speciation study of sulfur(IV) in aqueous solution. *Dalton Trans.* **43**, 2147–2152.

Bowles M. W., Mogollón J. M., Kasten S., Zabel M. and Hinrichs K.-U. (2014) Global rates of marine sulfate reduction and implications for sub-sea-floor metabolic activities. *Science* **344**, 889–891.

Bradley A. S., Leavitt W. D. and Johnston D. T. (2011) Revisiting the dissimilatory sulfate reduction pathway. *Geobiology* **9**, 446–457.

Brandt C. and van Eldik R. (1995) Transition metal-catalyzed oxidation of sulfur (IV) oxides. atmospheric-relevant processes and mechanisms. *Chem. Rev.* **95**, 119–190.

Brunner B. and Bernasconi S. M. (2005) A revised isotope fractionation model for dissimilatory sulfate reduction in sulfate reducing bacteria. *Geochim. Cosmochim. Acta* **69**, 4759–4771.

Canfield D. E. and Teske A. (1996) Late Proterozoic rise in atmospheric oxygen concentration inferred from phylogenetic and sulphur-isotope studies. *Nature* **382**, 127–132.

Canfield D. E. (2001) Biogeochemistry of sulfur isotopes. *Rev. Mineral. Geochem.* **43**, 607–636.

Canfield D. E. (2004) The evolution of the Earth surface sulfur reservoir. *Am. J. Sci.* **304**, 839–861.

Connick R. E., Tam T. M. and Von Deuster E. (1982) Equilibrium constant for the dimerization of bisulfite ion to form disulfite(2-) ion. *Inorg. Chem.* **21**, 103–107.

Eldridge D. L., Guo W. and Farquhar J. (2016) Theoretical estimates of equilibrium sulfur isotope effects in aqueous sulfur systems: highlighting the role of isomers in the sulfite and sulfoxylate systems. *Geochim. Cosmochim. Acta* **195**, 171–200.

Eriksen T. E. (1972) Sulfur isotope effects. I. The isotopic exchange coefficient for the sulfur isotopes 34S–32S in the system SO2g-HSO3-aq at 25, 35, and 45 °C. *Acta Chem. Scand.* **26**, 573–580.

Farquhar J., Wu N., Canfield D. E., Oduro H., Nanping W. U., Canfield D. E. and Oduro H. (2010) Connections between sulfur cycle evolution, sulfur isotopes, sediments, and base metal sulfide deposits. *Econ. Geol.* **105**, 509–533.

Frantz J. D., Dubessy J. and Mysen B. (1993) An optical cell for Raman spectroscopic studies of supercritical fluids and its application to the study of water to 500 °C and 2000 bar. *Chem. Geol.* **106**, 9–26.

Goldberg R. N. and Parker V. B. (1985) Thermodynamics of solution of SO₂(g) in water and of aqueous sulfur dioxide solutions. *J. Res. Natl. Bur. Stand. (1934)* **90**, 341–358.

Golding R. M. (1960) 741. Ultraviolet absorption studies of the bisulphite–pyrosulphite equilibrium. *J. Chem. Soc.*, 3711–3716.

Huang S.-L., Wu L.-C., Liang H.-K., Pan K.-T., Horng J.-T. and Ko M.-T. (2004) PGTdb: a database providing growth temperatures of prokaryotes. *Bioinformatics* **20**, 276–278.

Herlinger A. W. and Long T. V. (1969) Investigation of the structure of the pyrosulfite ion in aqueous solution using Raman and infrared spectroscopies. *Inorg. Chem.* **8**, 2661–2665.

Horner D. A. and Connick R. E. (1986) Equilibrium quotient for the isomerization of bisulfite ion from HSO3- to SO3H-. *Inorg. Chem.* **25**, 2414–2417.

Ishimoto M. and Fujimoto D. (1961) Biochemical studies on sulfate-reducing bacteria: X. Adenosine-5′-phosphosulfate reductase. *J. Biochem.* **50**, 299–304.

Johnston D. T., Farquhar J. and Canfield D. E. (2007) Sulfur isotope insights into microbial sulfate reduction : When microbes meet models. **71**, 3929–3947.

Johnston D. T. (2011) Multiple sulfur isotopes and the evolution of Earth's surface sulfur cycle. *Earth-Sci. Rev.* **106**, 161–183.

Jørgensen B. B., Bang M. and Blackburn T. H. (1990) Anaerobic mineralization in marine-sediments from the baltic-sea-north-sea transition. *Mar. Ecol. Ser.* **59**, 39–54.

Jørgensen B. B. (1977) The sulfur cycle of a coastal marine sediment (Limfjorden, Denmark). *Limn. Ocean.* **22**, 814–832.

Jørgensen B. B. (1982) Mineralization of organic matter in the sea bed – the role of sulphate reduction. *Nature* **296**, 643–645.

Jørgensen B. B. and Nelson D. C. (2004) Sulfide oxidation in marine sediments: Geochemistry meets microbiology. In *Special Paper 379: Sulfur Biogeochemistry - Past and Present.* Geological Society of America, pp. 63–81.

Kaplan I. R. and Rittenberg S. C. (1964) Microbiological fractionation of sulphur isotopes. *J. Gen. Microbiol.* **34**, 195–212.

Klenk H. P., Clayton R. A., Tomb J. F., White O., Nelson K. E., Ketchum K. A., Dodson R. J., Gwinn M., Hickey E. K., Peterson J. D., Richardson D. L., Kerlavage A. R., Graham D. E., Kyrpides N. C., Fleischmann R. D., Quackenbush J., Lee N. H., Sutton G. G., Gill S., Kirkness E. F., Dougherty B. A., McKenney K., Adams M. D., Loftus B., Peterson S., Reich C. I., McNeil L. K., Badger J. H., Glodek A., Zhou L., Overbeek R., Gocayne J. D., Weidman J. F., McDonald L., Utterback T., Cotton M. D., Spriggs T., Artiach P., Kaine B. P., Sykes S. M., Sadow P. W., D'Andrea K. P., Bowman C., Fujii C., Garland S. A., Mason T. M., Olsen G. J., Fraser C. M., Smith H. O., Woese C. R. and Venter J. C. (1997) The complete genome sequence of the hyperthermophilic, sulphate-reducing archaeon Archaeoglobus fulgidus. *Nature* **390**, 364–370.

Kobayashi K., Seki Y. and Ishimoto M. (1974) Studies on bacteria of sulfite reductase from desulfovibrio vulgaris-mechanism of trithionate, thiosulfate, and sulfide formation and enzymatic properties. *J. Biochem.* **75**, 519–529.

Leavitt W. D., Halevy I., Bradley A. S. and Johnston D. T. (2013) Influence of sulfate reduction rates on the Phanerozoic sulfur isotope record. *Proc. Natl. Acad. Sci. USA* **110**, 11244–11249.

Leavitt W. D., Bradley A. S., Santos A. A., Pereira I. A. C. and Johnston D. T. (2015) Sulfur isotope effects of dissimilatory sulfite reductase. *Front. Microbiol.* **6**, 1–20.

Li X., Gilhooly W. P., Zerkle A. L., Lyons T. W., Farquhar J., Werne J. P., Varela R. and Scranton M. I. (2010) Stable sulfur isotopes in the water column of the Cariaco Basin. *Geochim. Cosmochim. Acta* **74**, 6764–6778.

Littlejohn D., Walton S. A. and Chang S.-G. (1992) A Raman study of the isomers and dimer of hydrogen sulfite ion. *Appl. Spec.* **46**, 848–851.

Meyer B., Peter L. and Shaskey-Rosenlund C. (1979) Raman spectra of isotopic bisulfite and disulfite ions in alkali salts and aqueous solution. *Spectrochim. Acta Part A Mol. Spectrosc.* **35**, 345–354.

Millero F. J., Hershey J. P., Johnson G. and Zhang J.-Z. (1989) The solubility of SO_2 and the dissociation of H_2SO_3 in NaCl solutions. *J. Atmos. Chem.* **8**, 377–389.

Millero F. J. (1991) The oxidation of H_2S in Framvaren Fjord. *Limnol. Oceanogr.* **36**, 1007–1014.

Oliveira T. F., Vonrhein C., Matias P. M., Venceslau S. S., Pereira I. a. C. and Archer M. (2008) The crystal structure of Desulfovibrio vulgaris dissimilatory sulfite reductase bound to

DsrC provides novel insights into the mechanism of sulfate respiration. *J. Biol. Chem.* **283**, 34141–34149.

Parey K., Fritz G., Ermler U. and Kroneck P. M. H. (2013) Conserving energy with sulfate around 100 °C – structure and mechanism of key metal enzymes in hyperthermophilic Archaeoglobus fulgidus. *Metallomics* **5**, 302–317.

Parey K., Warkentin E., Kroneck P. M. H. and Ermler U. (2010) Reaction cycle of the dissimilatory sulfite reductase from archaeoglobus fulgidus. *Biochemistry* **49**, 8912–8921.

Peck H. D. (1962) The role of Adenosine-5'-phosphosulfate in the reduction of sulfate to sulfite by Desulfovibrio desulfuricans. *J. Biol. Chem.* **237**, 198–203.

Phillips J. C. (1984) Microscopic origin of anomalously narrow Raman lines in network glasses. *J. Non. Cryst. Solids* **63**, 347–355.

Rees C. E. (1973) A steady-state model for sulphur isotope fractionation in bacterial reduction processes. *Geochim. Cosmochim. Acta* **37**, 1141–1162.

Rickard D. (2014) The Sedimentary Sulfur System: Biogeochemistry and Evolution through Geologic Time. In *Treatise on Geochemistry.* Elsevier. pp. 267–326.

Risberg E. D., Eriksson L., Mink J., Pettersson L. G. M., Skripkin M. Y. and Sandström M. (2007) Sulfur X-ray absorption and vibrational spectroscopic study of sulfur dioxide, sulfite, and sulfonate solutions and of the substituted sulfonate ions $X3CSO3-$ (X = H, Cl, F). *Inorg. Chem.* **46**, 8332–8348.

Rudolph W. (1996) Structure and Dissociation of the Hydrogen Sulphate Ion in Aqueous Solution over a Broad Temperature Range: A Raman Study. *Zeitschrift für Phys. Chem.* **194**, 73–95.

Santos A. A., Venceslau S. S., Grein F., Leavitt W. D., Dahl C., Johnston D. T. and Pereira I. A. C. (2015) A protein trisulfide couples dissimilatory sulfate reduction to energy conservation. *Science* **350**, 1541–1545.

Shen Y. and Buick R. (2004) The antiquity of microbial sulfate reduction. *Earth-Sci. Rev.* **64**, 243–272.

Shen Y., Buick R. and Canfield D. E. (2001) Isotopic evidence for microbial sulphate reduction in the early Archaean era. *Nature* **410**, 77–81.

Shen Y., Farquhar J., Masterson A., Kaufman A. J. and Buick R. (2009) Evaluating the role of microbial sulfate reduction in the early Archean using quadruple isotope systematics. *Earth Planet. Sci. Lett.* **279**, 383–391.

Seifert F. A., Mysen B. O. and Virgo D. (1983) Raman-study of densified vitreous silica. *Phys. Chem. Glasses* **24**, 141–145.

Sim M. S., Bosak T. and Ono S. (2011a) Large sulfur isotope fractionation does not require disproportionation. *Science (80-)* **333**, 74–77.

Sim M. S., Ono S., Donovan K., Templer S. P. and Bosak T. (2011b) Effect of electron donors on the fractionation of sulfur isotopes by a marine Desulfovibrio sp. *Geochim. Cosmochim. Acta* **75**, 4244–4259.

Sim M. S., Paris G., Adkins J. F., Orphan V. J. and Sessions A. L. (2017) Quantification and isotopic analysis of intracellular sulfur metabolites in the dissimilatory sulfate reduction pathway. *Geochim. Cosmochim. Acta* **206**, 57–72.

Steudel R. and Steudel Y. (2009) Sulfur dioxide and water: structures and energies of the hydrated species $SO_2 \cdot nH_2O$, $[HSO_3]^- \cdot n\,H_2O$, $[SO_3H]^- \cdot nH_2O$, and $H_2SO_3 \cdot nH_2O$ (n = 0–8). *Eur. J. Inorg. Chem.* **2009**, 1393–1405.

Ueno Y., Ono S., Rumble D. and Maruyama S. (2008) Quadruple sulfur isotope analysis of ca. 3.5 Ga Dresser formation: new evidence for microbial sulfate reduction in the early Archean. *Geochim. Cosmochim. Acta* **72**, 5675–5691.

Wacey D., Kilburn M. R., Saunders M., Cliff J. and Brasier M. D. (2011) Microfossils of sulphur-metabolizing cells in 3.4-billion-year-old rocks of Western Australia. *Nat. Geosci.* **4**, 698–702.

Wing B. A. and Halevy I. (2014) Intracellular metabolite levels shape sulfur isotope fractionation during microbial sulfate respiration. *Proc. Natl. Acad. Sci.* **111**, 18116–18125.

Zhang J. Z. and Millero F. J. (1993) The chemistry of the anoxic waters in the Cariaco Trench. *Deep. Res. Part I* **40**, 1023–1041.

Zopfi J., Ferdelman T. G. and Fossing H. (2004) Distribution and fate of sulfur intermediates—sulfite, tetrathionate, thiosulfate, and elemental sulfur—in marine sediments. *Geol. Soc. Am. Spec. Pap.* **379**, 97–116.

Zopfi J., Ferdelman T. G., Jørgensen B. B., Teske A. and Thamdrup B. (2001) Influence of water column dynamics on sulfide oxidation and other major biogeochemical processes in the chemocline of Mariager Fjord (Denmark). *Mar. Chem.* **74**, 29–51.

Associate editor: Gleb S. Pokrovski